Drop Impact Dynamics: Splashing, Spreading, Receding, Bouncing. . .

A.L. Yarin

Faculty of Mechanical Engineering, Technion—Israel Institute of Technology, Haifa 32000, Israel; email: meralya@tx.technion.ac.il

Annu. Rev. Fluid Mech. 2006. 38:159–92

The *Annual Review of Fluid Mechanics* is online at fluid.annualreviews.org

doi: 10.1146/annurev.fluid.38.050304.092144

0066-4189/06/0115-0159$20.00

Key Words

crown formation, recoil, rebound, jetting, fingering, wettability, roughness, free rim, cusp formation, secondary droplets

Abstract

The review deals with drop impacts on thin liquid layers and dry surfaces. The impacts resulting in crown formation are referred to as splashing. Crowns and their propagation are discussed in detail, as well as some additional kindred, albeit non-splashing, phenomena like drop spreading and deposition, receding (recoil), jetting, fingering, and rebound. The review begins with an explanation of various practical motivations feeding the interest in the fascinating phenomena of drop impact, and the above-mentioned topics are then considered in their experimental, theoretical, and computational aspects.

1. INTRODUCTION

> "In the land of splashes, what the scientist knows as Inertia and Surface Tension are the sculptors in liquids, and fashion from them delicate shapes none the less beautiful because they are too ephemeral for any eye but that of the high-speed camera."
>
> –Edgerton & Killian (1954), slightly modified

Drop impacts on solid and liquid surfaces are a key element of a wide variety of phenomena encountered in technical applications, such as ink-jet printing, rapid spray cooling of hot surfaces (turbine blades, rolls in rolling mills for steel production, lasers, semiconductor chips, and electronic devices), annealing, quenching of aluminum alloys and steel, fire suppression by sprinklers, internal combustion engines (intake ducts of gasoline engines or piston bowls in direct-injection diesel engines), incinerators, spray painting and coating, plasma spraying, and crop spraying. Microfabrication of structured materials, solder bumps on printed circuit boards, and electric circuits in microelectronics produced by precision solder-drop dispensing, as well as liquid atomization and cleaning, and ice accumulation on power lines and aircraft also involve drop impacts. The latter are also important in criminal forensics, in development of nonwettable or fully wettable surfaces, in high-accuracy activation or passivation of substrates by microdrops, in transport of surface contaminants into bulk liquids, and in gas entrapment. Understanding the accompanying physical phenomena is of utmost importance in formulating reliable boundary conditions in numerical codes for spray simulation. Such large-scale and widespread natural phenomena as aeration of the surface layers of lakes, seas, and oceans depend on air bubble entrainment due to rain drop impacts. These impacts at ocean surfaces lead to formation of upward jets and secondary droplets, which evaporate and form salt crystals. The latter serve as nucleation sites in clouds, with the attendant relevance to meteorology. Erosion of soil, dispersal of spores and micro-organisms, and underwater noise during rains are three additional natural phenomena involving drop impact. Nail-like jets and bubbles are a familiar spectacle during rain falling on puddles and ponds.

Worthington (1908) was one of the first to investigate these impacts systematically and his book contains many fascinating photographs of the phenomena accompanying drop- and solid-ball impacts on deep liquid pools. In spite of its commonness, and of more than 100 years of research, the phenomenon is still far from being fully understood and continues to attract physicists, engineers, and mathematicians. It even attracts the general public and motivates potential customers, given the number of commercials based on drop impact scenes aired on television and shown on postcards (**Figure 1**).

The accompanying phenomena are extremely diverse, involved, and surprising. A drop may be spherical or elliptic (due to oscillations) at the moment of impact. It may impact on the free surface of a liquid in a deep pool, on a thin liquid film on a wall, or on a dry solid surface. The impact may be normal (perpendicular) or oblique, in air or in vacuum. The liquid may be Newtonian or non-Newtonian (e.g., a viscoelastic polymer or a surfactant solution). The liquids of the drop and

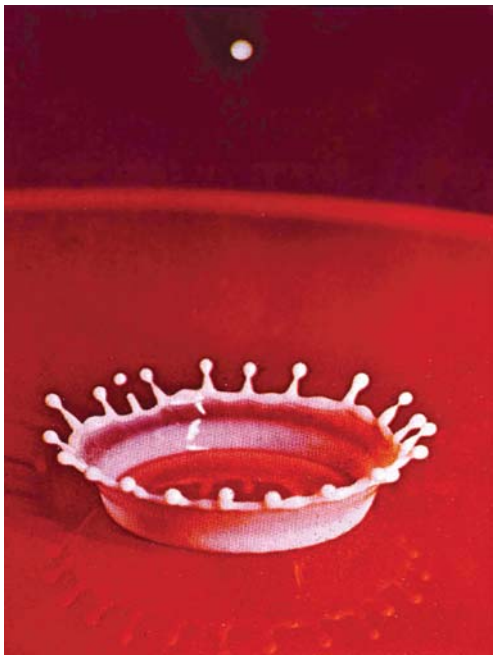

Figure 1

An American postcard with a famous Edgerton's photograph. Courtesy of Harold & Ester Edgerton Foundation (2005) and Palm Press, Inc.

pool/film may be miscible or immiscible. The solid surface may be hard or soft, rough or smooth, chemically homogeneous or heterogeneous. It may also be porous, flat or curved, at a temperature different from that of the drop or the same. On liquid surfaces, pre-existing or generated waves may affect the flow pattern. The impact may result in the drop spreading over the solid surface, receding, rebounding, or even levitating if the evaporation near a hot wall is sufficiently strong for the Leidenfrost effect. A crater may form in the liquid bulk in a pool and later on collapse, leading to formation of the so-called Worthington jet flowing out from its center and being subjected to capillary breakup. The impact on a liquid film may result in crown formation, propagation, and breakup, as well as in tiny bubble trapping, or—under certain conditions—noncoalescence and even rolling over the surface.

The outcome of drop impact depends on the impact velocity, its direction relative to the surface, drop size, the properties of the liquid (its density, viscosity, viscoelasticity, and some other non-Newtonian effects for rheologically complex fluids), the surface or interfacial tension, the roughness and wettability of the solid surface, the nonisothermal effects (e.g., solidification and evaporation), and air entrapment. In very strong impacts, liquid compressibility is also a factor. By contrast, following the impact of solid balls and projectiles onto armor plates in the hypervelocity range, the solid materials flow like fluids, and the influence of their elasticity, yield stress

and plasticity is negligible compared to inertial effects. As a result, phenomena such as frontal ejecta and crater formation in solid-solid impacts are reminiscent of those characteristic of liquid drop impact (i.e., splashing and crown formation), which led Worthington to call the former "permanent splashes." In cosmic-scale impacts of asteroids (a spectacular example of which is the Arizona Meteor Crater), material vaporization becomes a dominant factor.

The main dimensionless groups governing drop impact and employed in the present review are

$$\mathrm{We} = \frac{\rho \mathrm{D} \mathrm{V}_0^2}{\sigma}, \quad \mathrm{Re} = \frac{\rho \mathrm{D} \mathrm{V}_0}{\mu}, \quad \mathrm{Oh} = \frac{\mu}{(\rho \sigma \mathrm{D})^{1/2}} = \frac{\mathrm{We}^{1/2}}{\mathrm{Re}} \qquad (1a-c)$$

$$\mathrm{K} = \mathrm{We} \cdot \mathrm{Oh}^{-2/5}, \quad \mathrm{H} = \frac{\mathrm{h}_0}{\mathrm{D}}, \qquad (1d-e)$$

where ρ, μ, and σ denote liquid density, viscosity, and surface tension, respectively, D and V_0 the drop diameter and impact velocity, respectively, and h_0 the thickness of the pre-existing liquid film. We, Re and Oh denote the Weber, Reynolds, and Ohnesorge numbers, respectively, and H the dimensionless film thickness; K is an important composite group.

Gravity-related effects are characterized by the Bond number $\mathrm{Bo} = \rho g D^2/\sigma$, i.e., the ratio of D^2 to the square of the capillary length $(\sigma/\rho g)^{1/2}$ (g being gravity acceleration), or by the Froude number $\mathrm{Fr} = V_0{}^2/(gD) = \mathrm{We}/\mathrm{Bo}$. Note, however, that in the phenomena accompanying drop impact, gravity effects are typically not important. Further dimensionless parameters characterizing roughness and wettability effects are mentioned below, mostly in relation to drop impact on solid dry surfaces.

The abundance of phenomena accompanying and affecting drop impact makes it difficult to cover all of them in a comprehensive single review. Some topics have been covered separately in several previous reviews. For example, the compressibility effects in the impacts of water droplets of diameters $\sim$200 μm with velocities of about 100 m/s on solid surfaces were considered by Lesser & Field (1983) and Rein (1993). Under such conditions the Weber and Reynolds numbers are of the order of 10^4 to 10^5. Shock waves are expected to be created and then propagate over the impacting droplet. At a certain moment, the shock wave overtakes the moving contact line and spallation at the droplet bottom sets in (sometimes referred to as "jetting," but totally different from the jetting discussed in detail in the present review). The characteristic time of spallation is of the order of several nanoseconds.

Impact velocities resulting in compressibility effects with the corresponding characteristic times of the order of several nanoseconds are outside the scope of the present review, which is confined to the range $V_0 \approx 1$ to 30 m/s, at which compressibility effects in typical liquids are negligible.

Prosperetti & Oguz (1993) and Rein (1993) reviewed the phenomena accompanying the drop impact at moderate velocities of the order of 1 to 30 m/s on a deep pool. In this case the liquid motion initiated by the drop is virtually unconstrained and capable of pushing apart a significant liquid mass under the impact site. As a

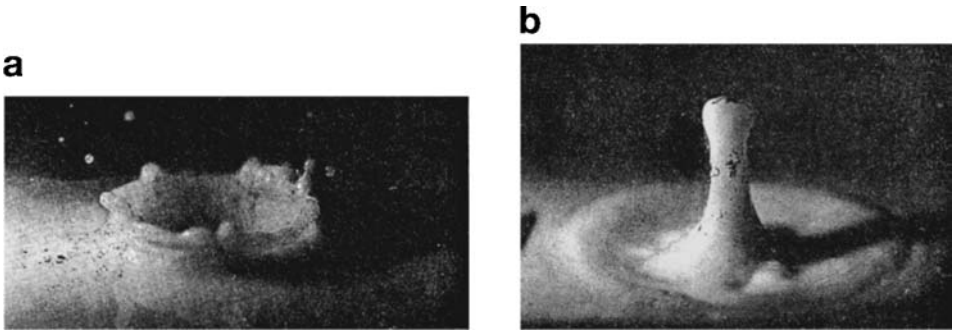

Figure 2

Water drop impact on a deep pool of milk mixed with water. (*a*) Crater surrounded by a crown-like ejecta at 40 ms after the impact. (*b*) Worthington jet rising from the collapsing crater at 116 ms. From Worthington (1908).

result, an almost hemispherical crater appears initially below the unperturbed surface level. The crater is surrounded by a rather thick rim of displaced liquid (sometimes referred to as a corona or crown, cf. **Figure 2*a***). Its expansion is transitory because the surface tension arrests the downward motion of the liquid at a certain crater size, at which the latter collapses and the motion is reversed. Depending on the primary impact strength, the collapse may restore the plane free surface after several oscillations due to the competition of the surface tension and inertia, or induce ejection of a Worthington jet in the middle of the crater (**Figure 2*b***). Sometimes sections of the crater walls merge during its collapse, resulting in entrapment of a single or several bubbles in the liquid bulk. Under certain impact conditions vortex rings are formed in the pool.

The phenomena accompanying drop impact on a deep liquid pool are not considered in the present review, which deals primarily with thin liquid layers (compared to the drop diameter) and dry solid surfaces, except for occasional references to relevant results on drop- and solid-body impacts on deep liquid pools. The liquids of interest are mostly Newtonian, with impact velocities of the order of $V_0 \sim 1$ to 30 m/s and drop diameters typically $D \sim 100$ to 3000 μm, with occasional references to certain non-Newtonian effects characteristic of the impact of rheologically complex liquids.

The review is organized as follows. The experiments on splashing and crown formation and propagation due to drop impact on thin liquid layers are considered in Section 2. The corresponding theoretical and numerical works are reviewed in Section 3. Additional kindred phenomena, including jetting, bubble encapsulation in thin liquid films, drop spreading, and self-similar capillary waves are discussed in Section 4. Experimental results on drop impacts on dry solid surfaces are considered in Section 5, which covers spreading, fingering, splashing, receding, and rebound. Section 6 is devoted to theoretical and numerical modeling of drop impact on a solid dry surface. Conclusions are drawn in Section 7, where some open questions and future directions are also mentioned.

2. EXPERIMENTS ON DROP IMPACT ON A THIN LIQUID LAYER, AND THE DEFINITION OF SPLASHING

This section deals with the situation involving pre-existing liquid films, or films created by impacts of previous drops. Normal impact of successive monodisperse ethanol drops (with $D = 70$–340 μm and V_0 up to 30 m/s) on a solid surface was studied experimentally by Yarin & Weiss (1995). Following the first impact, the wall was permanently covered by a thin liquid film with thickness of the order of $h \approx (\nu/f)^{1/2}$, f being the frequency of the impacts and f^{-1} the characteristic time of one impact. For $f \sim 10^4$ s^{-1} and kinematic viscosity $\nu \sim 10^{-6}$ m^2/s, the values of h were in the range of 20–50 μm, typically with $h/D \approx 1/6$. The film thickness was sufficiently large relative to the mean surface roughness (1 or 16 μm). The experiments revealed two characteristic flow patterns on the surface, illustrated in **Figure 3**. At sufficiently low impact velocities the drops spread over the wall, taking the shape of lamellae with a visible outer rim (**Figure 3*a***). At still lower impact velocities practically no rim is visible, which Rioboo et al. (2003) termed deposition. By contrast, at higher impact velocities the lamellae later took the shape of crowns (**Figure 3*b***) consisting of a thin liquid sheet with an unstable free rim at the top, from which numerous small secondary droplets were ejected. Only the impact patterns of the type shown in **Figure 3*b*** are called splashing in the present review, whereas those of the type shown in **Figure 3*a*** are referred to as spreading. Several other definitions of splashing can be found in the literature. One example is liquid ejection from the crater in a deep pool, with or without formation of droplets at its rim (cf. **Figure 2*a***); another is formation of a Worthington jet ejected at the crater center (cf. **Figure 2*b***). These phenomena do not occur after impacts on the pre-existing thin liquid films of thickness h_0 with $H = h_0/D < 1$ (Rioboo et al. 2003, Wang & Chen 2000), and hence are not considered here. Drop spreading after an impact at a dry surface can be accompanied by instability at the

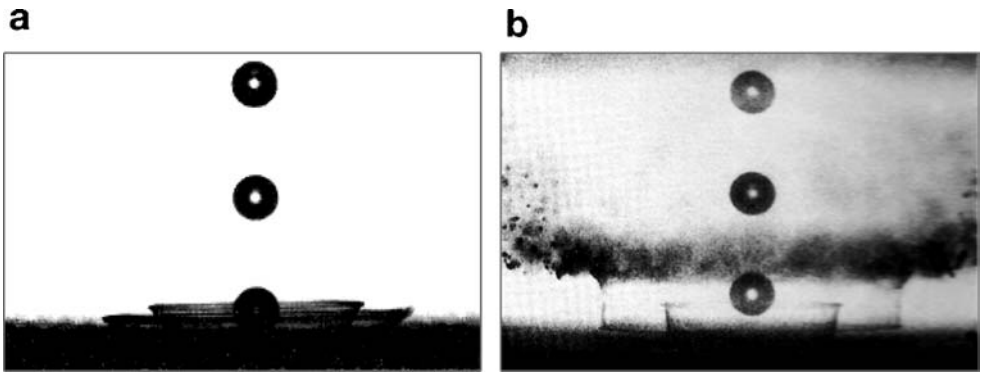

Figure 3

(*a*) Spreading ethanol drops stroboscopically illuminated. Spreading lamellae at two different stages can be recognized. Drop diameter $D = 279$ μm, impact velocity $V_0 = 7.8$ m/s, $We = 588$, $Re = 1409$, $Oh = 1.72 \cdot 10^{-2}$. (*b*) Splashing ethanol drops illuminated by a single flash. Drop diameter $D = 276$ μm, impact velocity $V_0 = 12.7$ m/s, $We = 1542$, $Re = 2270$, $Oh = 1.73 \cdot 10^{-2}$. From Yarin & Weiss (1995). Courtesy of Cambridge University Press.

outer rim of the liquid lamella, which is also sometimes referred to as splashing. In the present review this latter phenomenon is considered in Section 5 and is called fingering.

The experimental threshold velocity for drop splashing in a train of frequency f established by Yarin & Weiss (1995) is

$$V_{0S} = 18 \left(\frac{\sigma}{\rho} \right)^{1/4} \nu^{1/8} \, f^{3/8} \tag{2}$$

Drop spreading occurs at the impact velocities $V_0 < V_{0S}$, whereas at $V_0 > V_{0S}$ splashing and formation of a crown and multiple secondary droplets occur, as in **Figure 3*b***. Here and hereinafter the subscript S denotes the splashing threshold. It is remarkable that the drop diameter D has no effect on the splashing threshold. This implies that the crown originates from the liquid lamella at the surface long after the memory of the squashed primary drop has faded. This fact could be utilized for modeling (cf. Section 3). Due to the small scales involved, only inertia and surface tension are significant factors (with viscosity involved only via the film thickness), whereas the role of gravity is negligible. By contrast, in hydraulic jumps, even small-scale ones—i.e., in the radially spreading water films created by the impinging jets in kitchen sinks—gravity is the main driving force, although surface tension must be considered (Bush & Aristoff 2003). Splashing and hydraulic jumps are totally distinct phenomena.

Single-drop impacts on pre-existing films of the same liquid were studied by Cossali et al. (1997), Wang & Chen (2000), and Rioboo et al. (2003). In all these cases, crown formation, i.e., splashing, was recorded at sufficiently high impact velocities. For single impacts the ratio D/V_0 can play the role of the characteristic impact time, thus replacing f^{-1} for impacts in train (Yarin & Weiss 1995). Moreover, for thin pre-existing liquid films the film thickness h_0 might play a less important role than that of the layer stopped by the viscous forces at the wall $h \sim (\nu D/V_0)^{1/2}$. Then the splashing threshold (Equation 2) with $f \sim V_0/D$ could hold for a single impact. Using the dimensionless groups of Equation 1, we recast Equation 2 as $We_S \cdot Oh^{-2/5} \sim 10{,}396$. Therefore, a unique dimensionless group $K = We \cdot Oh^{-2/5}$ might govern the splashing threshold of a single impact on a pre-existing liquid film. Cossali et al. (1997) established experimentally the condition of drop splashing on pre-existing liquid films in the form

$$K > K_S = 2100 + 5880\, H^{1.44} \tag{3a}$$

$$0.1 < H < 1, \quad Oh > 7 \cdot 10^{-3} \tag{3b}$$

The threshold value on the right-hand side in Equation 3*a* was established for a specific value of the nondimensional roughness $R_{nd} = R_a/D = 5 \cdot 10^{-5}$, R_a being the roughness amplitude. A higher roughness affects the flow in extremely thin liquid lamellae on the surface, and the threshold value of K_S decreases (Cossali et al. 1997). The data of Wang & Chen (2000) and Rioboo et al. (2003) for low-viscosity liquids are also in reasonable agreement with Equation 3*a*. The latter authors showed that the parameter K may also be used to characterize transition from deposition to spreading with a visible rim. For $0.08 \leq H \leq 0.14$ it occurs at $K \approx 400$.

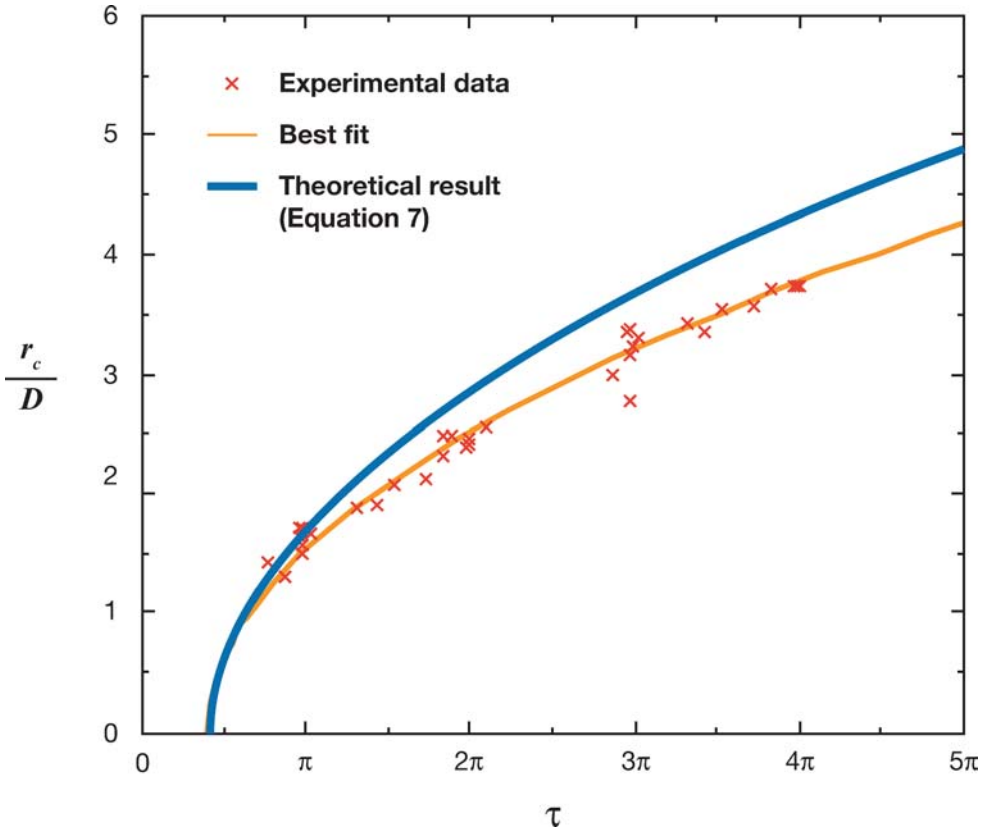

Figure 4

Radial position of crown's rim as a function of dimensionless time $\tau = 2\pi ft$. Experimental data indicated by red crosses; best fit by fine orange line; curve predicted by the theory (Equation 7) by bold blue line. Data obtained with ethanol drops with $D = 271\ \mu m$, $V_0 = 12.5$ m/s, $f = 19.973$ kHz, $We = 1467$, $Re = 2194$, $Oh = 1.75 \cdot 10^{-2}$. From Yarin & Weiss (1995). Courtesy of Cambridge University Press.

In splashing regimes crowns formed after a normal drop impact on a thin liquid layer propagate radially outward. The crown motion was recorded by Yarin & Weiss (1995) and an example of the experimental data is shown in **Figure 4**. The best-fit approximation of the data in **Figure 4** (the fine line) is

$$\frac{r_c}{D} = 1.12\,(\tau - 1.28)^{1/2} \tag{4}$$

where r_c is the crown radial position and $\tau = 2\pi ft$ is dimensionless time. Analysis of the corresponding data of Levin & Hobbs (1971) and Cossali et al. (1997) for a single impact on thin pre-existing liquid layers also reveals square-root dependence of r_c on time. Cossali et al. (2004) reported the exponent value of 0.43 instead of 1/2. Elsewhere, Sivakumar & Tropea (2002) found the dependence $r_c \sim T^{0.2}$ with $T = tV_0/D$ in their experiments with splashing impacts in sprays. The reason for the much

weaker dependence of r_c on time in the latter case is mutual interaction of the crowns produced by neighboring drop impacts. Where these interactions were insignificant, the crown heights h_c increased linearly with r_c, at a rate of $dh_c/dr_c = 0.57$ (Yarin & Weiss 1995). Cossali et al. (2004) provided experimental data on crown wall thickness ($\delta \sim 0.2D$) and height as functions of time.

Flash illumination of a crown reveals the details of secondary droplet formation there. The photographs by Levin & Hobbs (1971) and Yarin & Weiss (1995), combined in **Figures 5*a*** and ***b***, show a free rim on the crown top with multiple thin jets emerging from its cusps. These jets break up into droplets due to the capillary breakup

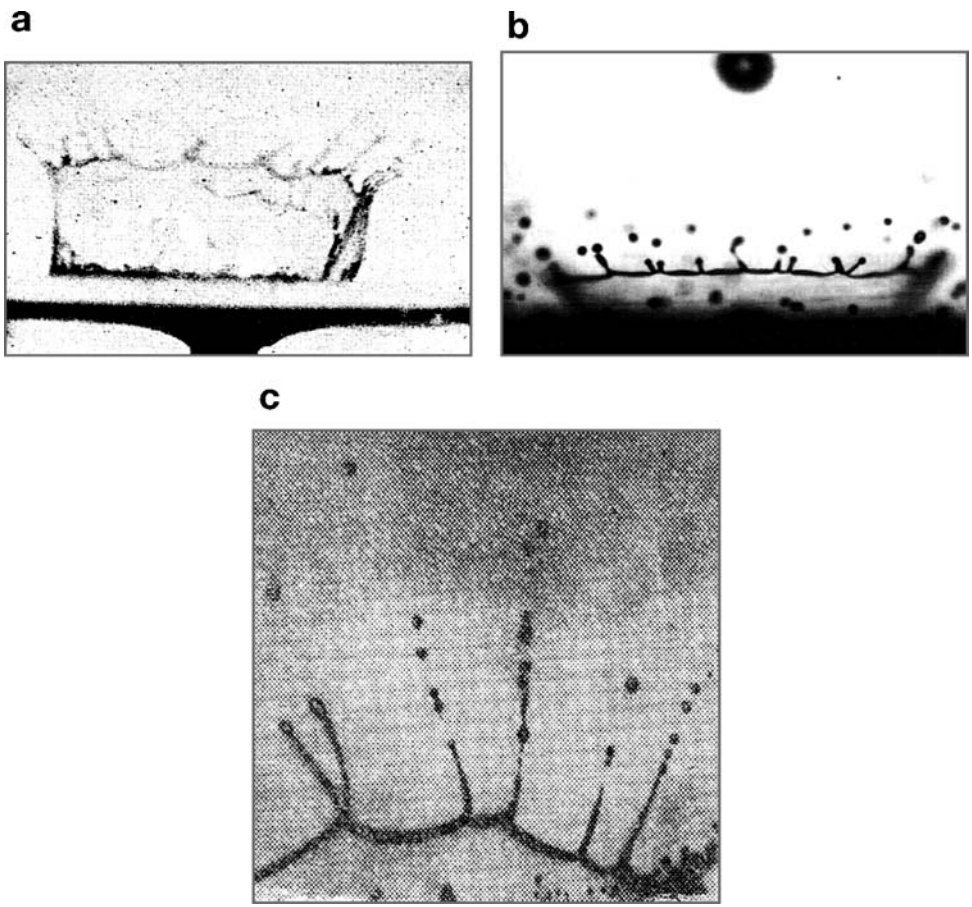

Figure 5

Free rim, jets originating from the cusps, and secondary droplet formation. (*a*) Splashing of a single water drop at a pre-existing liquid layer. $D = 2.9$ mm, $V_0 = 4.8$ m/s, $h_0 = 0.5$ mm, $We = 928$, $Re = 13{,}920$, $Oh = 2.2 \cdot 10^{-3}$, and $H = 0.172$, 1.8 ms after the impact. From Levin & Hobbs (1971). Courtesy of the Royal Society of London. (*b*) Splashing of an ethanol drop in a train, corresponding to those of **Figure 3*b***. From Yarin & Weiss (1995). Courtesy of Cambridge University Press. (*c*) Breakup of a soap bubble, photographed by M.O. Kornfeld.

mechanism. This is a good illustration of the general fact that a two-dimensional (2D) liquid sheet is broken by surface tension (but not directly, because the surface energy in fact increases) through rearrangement into a free rim at the edge (Taylor 1959). When disturbed, a rim on any liquid film inevitably forms cusps (Yarin 1993; cf. **Figure 5*c***). Rozhkov et al. (2002) photographed similar free rims with cusps and jets originating in them on free liquid lamellae formed by drops impacting small targets. The cusps become the sites where the practically one-dimensional (1D) jets are squeezed out, thereby undergoing capillary breakup. Thus, the mechanism leading to secondary droplet formation in splashing is, in fact, multistage rearrangement of a 2D continuum (liquid sheet in the crown wall) into a 1D one (thin jets on the crown top). A sketch of the splashing mechanism is presented in **Figure 6**. Detailed experimental

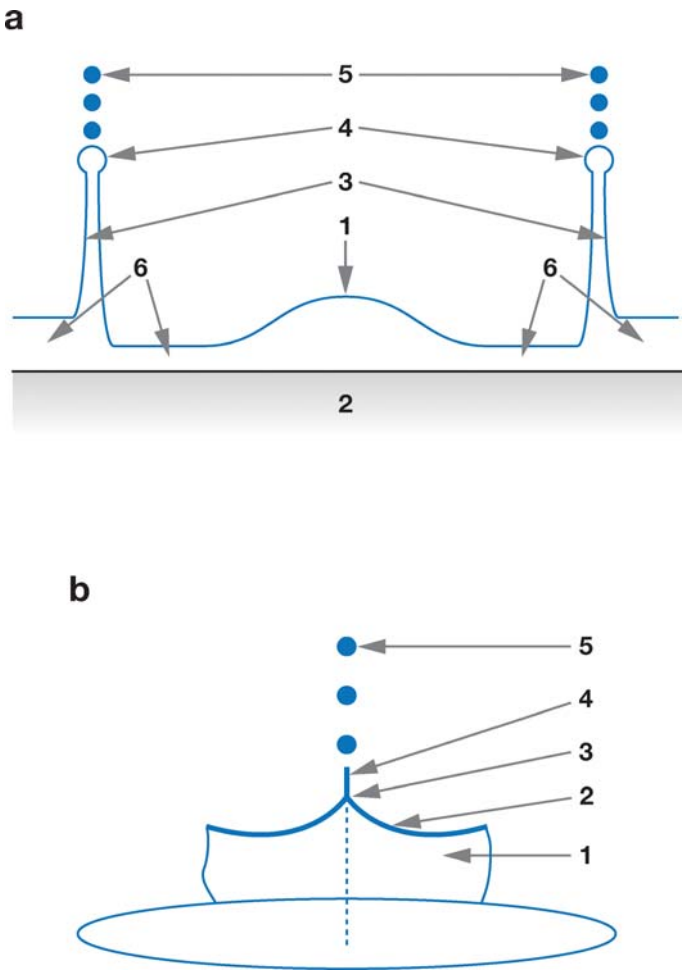

Figure 6

(*a*) Sketch of splashing mechanism: 1, residual top of impacting drop; 2, wall; 3, section of crown-like sheet propagating outward; 4, cross-section of free rim; 5, secondary droplets formed from cusps of free rim; 6, liquid layer on wall. (*b*) Free rim and secondary droplets magnified; 1, crown-like sheet; 2, free rim at its top edge; 3, cusp; 4, thin jet emerging at cusp; 5, secondary droplets formed on breakup of jet. From Yarin & Weiss (1995). Courtesy of Cambridge University Press.

information on the number of jets and secondary droplet sizes on the crown top is available in Cossali et al. (2004).

3. MODELING OF SPLASHING AT DROP IMPACT ON A WETTED SURFACE

At first glance, the real pattern of drop splashing in a train appears too complicated for any theoretical tools except the numerical ones. However, the fact that the crown originates from the liquid lamella at the surface after the impinging drop has already been squashed indicates that the underlying mechanism is relatively simple and its description could be based on a quasi-1D model. Such a model (Yarin & Weiss 1995) considers the situation where, after the drop impact, a circular spot near the lamella center has a distribution of the initial outward velocity of the order of the impact velocity V_0. The liquid moving outward from this central spot impinges on the surrounding liquid in the lamella. Because the liquid is incompressible, formation of an ordinary shock wave due to inward collapse of the material elements (in the gas-dynamical sense) is ruled out. However, if the condition

$$V_0 \gg \left(\frac{\sigma}{\rho}\right)^{1/4} \nu^{1/8} f^{3/8} \tag{5}$$

holds for a drop train impact, surface tension is totally dominated by inertia (if $f = V_0/D$ as for single drop impact, Equation 5 is equivalent to $K = WeOh^{-2/5} \gg 1$). As a result, due to the presence of the free surface, a kinematic discontinuity in the velocity distribution emerges, which is reminiscent of a shock wave in an incompressible liquid. Then, the liquid from the central spot moving along the surface and impinging onto the surrounding liquid at rest is propelled upward as a thin layer (the crown). The discontinuity propagates toward the thicker section of the film at the surface, detaching part of it in the manner of a cutter and propelling it into the crown. The theoretical splashing threshold (Equation 5) fully agrees with the experimental one (Equation 2).

The theory also predicts the crown position as it moves outward, as per

$$\frac{r_c}{D} = \frac{V_0^{1/2}}{6^{1/4}\pi^{1/2}\nu^{1/8}D^{1/4}f^{3/8}}(\tau - \tau_0)^{1/2} \tag{6}$$

where the dimensionless shifting time $\tau_0 = 2\pi f t_0$ is similar to the "polar distance" required for comparison of self-similar solutions for laminar and turbulent jets with experimental data. For the conditions corresponding to **Figure 4**, Equation 6 yields

$$\frac{r_c}{D} = 1.29\,(\tau - 1.28)^{1/2} \tag{7}$$

which is compared to the experimental data and their best fit, Equation 4, in **Figure 4** (the bold curve). Agreement is fairly close, except that the theoretical values of the ratio r_c/D exceed the experimental ones, due to the exclusion of the viscous losses at the moment of impact.

For a single impact on a thin pre-existing liquid layer of thickness h_0, the crown position is given by

$$\frac{r_c}{D} = \left(\frac{2}{3}\right)^{1/4} \frac{V_0^{1/2}}{D^{1/4} h_0^{1/4}} (t - t_0)^{1/2} \tag{8}$$

with t_0 being the shifting time. Equation 8 describes the experimental data of Levin & Hobbs (1971) fairly well, with an overestimate of about 10%, which is similar to the accuracy of Equations 6 and 7 versus the data in **Figure 4**.

Trujillo & Lee (2001) generalized the theory to account for the viscous losses. Their predictions, however, are rather close to those of Yarin & Weiss (1995), which indicates that crown formation and propagation are dominated by liquid inertia. Roisman & Tropea (2002) generalized the theory of Yarin & Weiss (1995) to allow for prediction of the crown wall thickness and shape for both normal and oblique drop impact on a liquid film on the wall. Predicted crown heights were in good agreement with the experimental data for thin liquid films with $H \leq 0.29$ (Cossali et al. 2004, Roisman & Tropea 2002). The same approach was used to model crown-crown interaction after the splashing of two neighboring drops in a spray (Roisman & Tropea 2002).

Fedorchenko & Wang (2004) proposed to calculate the crown angle relative to the liquid layer on the surface using the assumption that the crown rises tangentially to the impacting drop contour. This assumption is grounded in the works on penetration of convex rigid bodies into a deep fluid pool. It can hardly be justified for liquid drop impacts because the drops can deform, which results in jetting (see Section 4). Thus, it is not surprising that the theory based on it disagrees with experimental data: For example, in the case shown in **Figure 3*b***, the theory predicts an angle of 44° to 74° for a liquid layer thickness at the wall of 20 to 50 μm, whereas the visible crown angle is actually close to 90°.

Crown formation in splashing was demonstrated numerically in Weiss & Yarin (1999), where in strong impacts of single drops with $We \gtrapprox 40$ at timescales of the order of $t = 10^{-3}$ to 10^{-2} s crowns were formed and propagated over liquid films on a wall. In these calculations, the liquid in the drop and film was assumed to be inviscid, and the potential flow problem was solved using the boundary element method with the corresponding boundary integral equation. Davidson (2002) published kindred results obtained with an improved regridding procedure. According to the threshold condition (Equation 3), if it were to hold for any viscosity, an inviscid liquid should inevitably splash because $K = \infty$. This, however, does not occur in the simulations, probably because the numerical methods employed inevitably produce an artificial "scheme" viscosity. Propagation of the crowns in time of the order of $\sim 10^{-2}$ s (Davidson 2002, Weiss & Yarin 1999) very accurately followed the prediction of the analytical theory (Equation 8) and agreed with the experimental data of Cossali et al. (1997). The square-root law (Equation 8) was also supported by numerical simulations of a single impact on a thin liquid layer based on the Navier-Stokes equations solved by the volume-of-fluid method (Rieber & Frohn 1999). In these remarkable simulations, in the three cases shown in **Figure 7**, the Weber numbers were chosen above the splashing threshold of Equation 3. As a result, crowns were

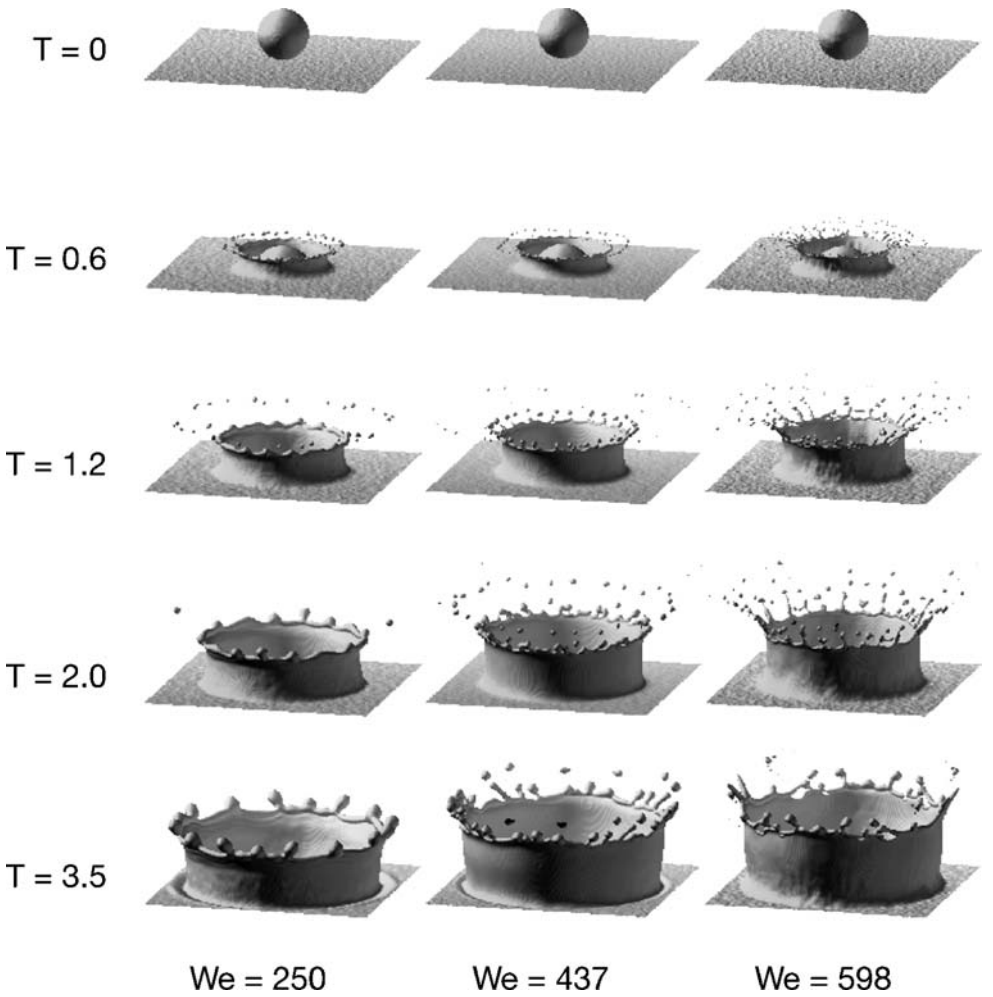

Figure 7

Direct numerical simulations of splashing based on the Navier-Stokes equations. Three cases of crown formation and propagation with We = 250, 437, and 598 with H = 0.116, 0.1, and 0.116, respectively. From Rieber & Frohn (1999). Courtesy of Elsevier.

formed and propagated outward, in full agreement with the results of the analytical theory.

Crown propagation is predicted to be preceded by capillary waves (Weiss & Yarin 1999, Yarin & Weiss 1995). The feature is observed in experiments: p. 111 in Edgerton & Killian (1954) and figure 5 in Cossali et al. (1997).

The free rim at the crown top is formed and propagates over the crown wall with the speed $V_{rim} = [2\sigma/(\rho\delta)]^{1/2}$, δ being the wall thickness (Taylor 1959). Formation of secondary droplets at the crown top is frequently attributed to one of two

theories. (*a*) The capillary instability of the free rim, which is considered as a toroidal thread and assumed to be fully detached from the crown (Mundo et al. 1995, Range & Feuillebois 1998) or attached to it (Fullana & Zaleski 1999). (*b*) Yarin & Weiss (1995) argued, however, that this mechanism significantly underpredicts the number of secondary droplets breaking up simultaneously on the crown top in their own and in Levin & Hobbs' (1971) experiments, and accordingly attributed secondary droplet formation to the bending perturbations of the toroidal rim. These perturbations could be triggered, for example, by the wall roughness at the moment a liquid element is propelled into the crown. Then the crown rim shape $y = Y(x, t)$ is governed by the eikonal equation (Roisman & Tropea 2002, Yarin & Weiss 1995)

$$\frac{\partial Y}{\partial t} = V_{rim}\left[1 + \left(\frac{\partial Y}{\partial x}\right)^2\right]^{1/2} \tag{9}$$

y being the coordinate directed along the crown wall toward the solid wall and x the circumferential coordinate over the crown wall.

The solution of Equation 9 shows that a perturbed rim always evolves into a cusped shape at any section where it was initially convex upward. At the cusp sites two neighboring sections of the free rim impinge on each other, squeezing a thin jet directed upward from the crown. The jets are subjected to capillary instability, which leads to formation of multiple secondary droplets. By contrast, Rieber & Frohn (1999) claimed that for the conditions considered in their simulations, as per **Figure 7**, it was the capillary instability of the crown top rim that was the driving mechanism of secondary droplet formation. Note that formation of secondary droplets was triggered in their simulations by adding specific random perturbations and did not occur without them. These authors reported holes in the crown wall under the top rim (visible in the cases with $We = 437$ and 598 in **Figure 7**), which are not typically observed experimentally. [Note, however, that Range & Feuillebois (1998) tried such an interpretation regarding one of their experiments with impact on thin liquid films; see also Roisman & Tropea (2005).] Thus, the predicted flow pattern close to the rim, which directly affects its breakup, could lead to nonphysical predictions related to the mechanism of secondary droplet formation. Note also that Fullana & Zaleski (1999) studied stability of a growing free rim at the edge of a liquid sheet and showed that this time-dependent basic flow does not result in capillary instability. The latter fact effectively rules out mechanism (*a*) as the reason for secondary droplet formation on top of the crown.

4. ADDITIONAL KINDRED PHENOMENA: JETTING, BUBBLE ENCAPSULATION, SPREADING, AND SELF-SIMILAR CAPILLARY WAVES

Drop impact on a layer provides an additional example of development of kinematic discontinuity (reminiscent of shock waves) in an incompressible liquid with a free surface. Weiss & Yarin (1999) predicted that at the initial moments of strong impacts ($We \gtrapprox 40$) at $t \sim 10^{-6}$ to 10^{-5} s, which is three orders of magnitude less than the time

of crown formation, jetting sets in the middle of the neck between the oncoming drop and the liquid layer. The numerical simulations of Davidson (2002) with an improved regridding procedure confirmed this result, and Josserand & Zaleski (2003) discussed the accompanying viscous effects. The jetting stems from the fact that under the inertia-dominated regime of impact, rapidly moving liquid in the upper part of the neck, brought by the drop, impinges on slowly moving liquid below. As a result, the oncoming liquid is pushed outward through the free surface as a radial liquid jet. This means that the velocity jump is so pronounced at We $\gtrapprox$ 40 that the inertial forces dominate the surface tension and squeeze liquid radially from the neck. Thus, the physical origin of the jetting is the same as that of crown formation: onset of a kinematic discontinuity irrespective of the specific shape of the free surface. The velocity of the jet tip was predicted to be significantly higher than the impact speed. The jet tip may reattach to the free surface of the layer at the surface, which results in entrapment of a torus-like bubble (at 40 $\lessapprox$ We $\lessapprox$ 1000). Alternatively, the jet tip may pinch off before reattachment (**Figure 8*a***), leading to formation of a liquid torus (at We $\gtrapprox$ 1000). This toroidal bubble is broken up by capillary instability into tiny bubbles (size about 10^{-3} D) over the time interval of the order of 10^{-6} s from the moment of formation. Similarly, the liquid torus breaks up into tiny droplets of similar size over an interval of the order of 10^{-6} s. Recognizing that the extremely

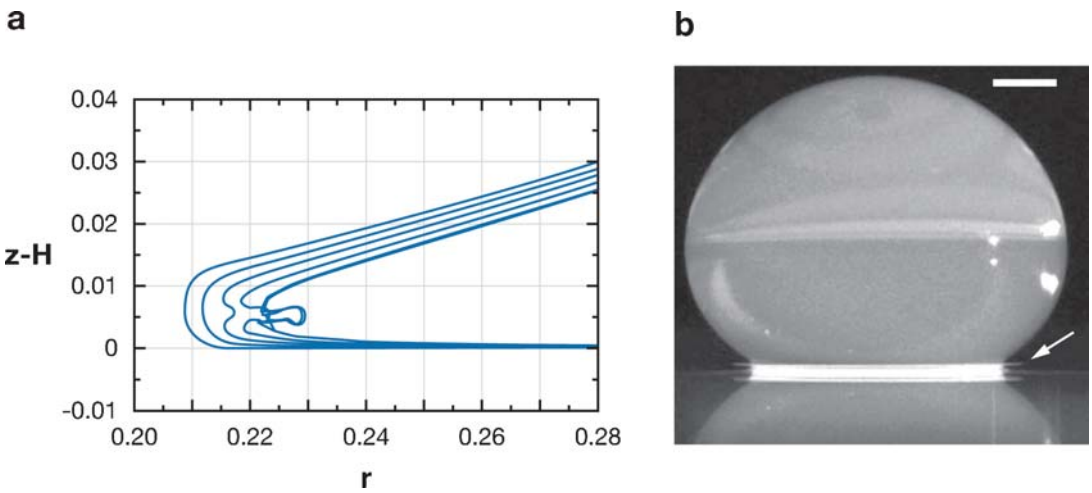

Figure 8

(*a*) Evolution of the free surface in the case of We = 2000, H = 0.125. The different curves correspond from left to right to times 0.1×10^{-4}, 2×10^{-4}, 3×10^{-4}, 4×10^{-4}, and 4.1×10^{-4}, rendered dimensionless by an arbitrary timescale $[D/(2g)]^{1/2}$, which is about 10^{-2} s for D = 2 mm. The solid wall is at z = 0, i.e., at z-H = −0.125 (z and the radial coordinate r are rendered dimensionless by D/2). The leading part of the jet pinches off a part of its bulk before it reconnects with the pre-existing film. From Weiss & Yarin (1999). (*b*) The jetting emerging from underneath the drop at We = 4170, Re = 1080, Oh = 0.0598, K = 12,866, and H = 0.952, i.e., above the splashing threshold of Equation 3 but long before crown formation. The arrow points to the radial liquid jet; the scale bar is 1-mm long. From Thoroddsen (2002). Courtesy of Cambridge University Press.

short times of the order of 10^{-6} to 10^{-5} s, and small dimensions of the order of 10^{-3} D $\sim$ 1 to 10 μm for D = 2 mm, are involved, Weiss & Yarin (1999) believed that the predictions could not be readily amenable to experimental verification. However, Thoroddsen (2002) did verify them in his amazing experiments (**Figure 8*b***). His measurements also revealed another striking result: The velocities of the jet tip are very high, of the order of 50 to 60 m/s, i.e., more than tenfold the impact velocity. He also studied evolution of these ejecta jets in detail.

Weiss &Yarin (1999) also mentioned that due to the same causes, similar jetting is encountered in the neck below a solid body penetrating an incompressible liquid. The most recent example was demonstrated by Thoroddsen et al. (2004). Using a novel ultra-high-speed video camera, they recorded jets emerging from the neck underneath a solid sphere ($We > 10^4$, $5 \cdot 10^2 \leq Re \leq 6 \cdot 10^5$) about 10^{-5} s after the impact. The jetting velocities were up to 300 m/s with no compressibility effects. The jetting swallows up to 90% of the impact energy and is responsible for the impact force.

Radial jetting kindred to splashing is not restricted to drop impacts. It was also found in free-water jets of relatively large radius with strong pulsations in the issue velocity imposed by a piston (Meier et al. 1992; cf. **Figure 9**). In such thick jets inertial forces dominate the surface tension. A segment of a jet issuing under a higher pressure than its predecessor moves faster and impinges on the slower-moving segment ahead. As a result, a kinematic discontinuity is formed in the longitudinal velocity distribution and radial jetting sets in. In **Figure 9**, liquid disks illustrate this, making the jets similar to a shish kebab. The phenomenon is equivalent to splashing due to drop impact, both physically and formally, provided the quasi-1D equations of liquid-jets dynamics are used (Yarin 1993).

A head-on collision of two liquid jets yields an additional example of splashing in the form of a radially expanding liquid sheet.

According to the bubble encapsulation mechanism, the toroidal bubble almost immediately breaks up into tiny bubbles spread over a ring surrounding the impact center. Micron-size bubbles appearing at 10^{-6} s are not readily amenable to experimental

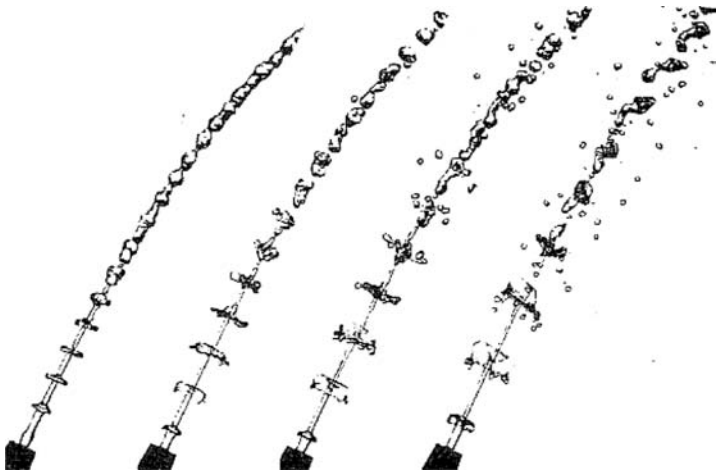

Figure 9

Jets issuing due to modulated pressure develop periodic radial jetting. Several modulation frequencies are of the order of 50 Hz; pressure amplitude modulation is more than 50%. From Meier et al. (1992). Courstesy of Springer Science and Business Media.

detection. However, in the experiments of Chandra & Avedisian (1991) with drops impinging on a hot surface, a bubble ring is seen (cf. their figure 6). The fact that such an ordered bubble ring emerges at temperatures below the boiling point may be related to the liquid evaporating into the micron-size bubbles, which enlarges them.

At We $\lessapprox$ 40, impacts can be characterized as weak. The numerical simulations of Weiss & Yarin (1999) and Davidson (2002) showed that under the action of the surface tension, whose role in weak impacts is prominent, the whole axisymmetric neck between the drop and the pre-existing liquid film moves outward without jetting, and the accompanying capillary waves at the initial moments (of the order of 10^{-5} s) are reminiscent of those found by Oguz & Prosperetti (1989). In the axisymmetric simulations, where only liquid/liquid impact in vacuum was considered, the opposite volumes of liquid never touched, thus bubble encapsulation similar to the "Messler entrainment" simulated and explained (in relation to their planar case) by Oguz & Prosperetti (1989) was not observed. The presence of air, however, affects the situation dramatically (Thoroddsen et al. 2003). On the timescale of about 10^{-4} to 10^{-3} s, an air lens may be entrapped between an oncoming drop and the liquid layer. The lens evolves according to the above predictions of Oguz & Prosperetti (1989), the air finds itself locked in a toroidal bubble, and the capillary instability leads to the formation of tiny bubbles located on a ring ("necklace instability," according to Thoroddsen et al. 2003). Coalescence of a drop deposited gently onto the free surface of a layer of the same liquid can be accompanied by a cascade of pinching events (Thoroddsen & Takehara 2000).

For weak impacts on a wetted surface, the base radius R of a drop is initially determined by inertia and surface tension and evolves as $R \sim (\sigma D/\rho)^{1/4} t^{1/2}$ (Biance et al. 2004). At much longer times, of the order of 10^{-2} s, weak impacts produce spreading patterns. A doughnut-like wave with a rim as shown in **Figure 10** represents

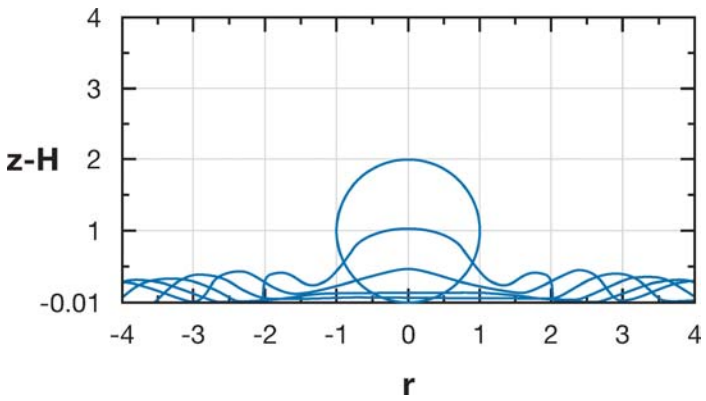

Figure 10

Drop spreading. Evolution of the free surface in the case of We = 20, H = 0.01. The different curves correspond to times 0, 0.1, 0.2, 0.3, 0.4, 0.5, and 0.6. There is no crown formed because the inertial effects are relatively weak compared to the capillary ones. As a result, the drop gradually spreads over the pre-existing liquid layer. Time and the coordinates are rendered dimensionless, as in **Figure 8*a***. From Weiss & Yarin (1999). Courtesy of Cambridge University Press.

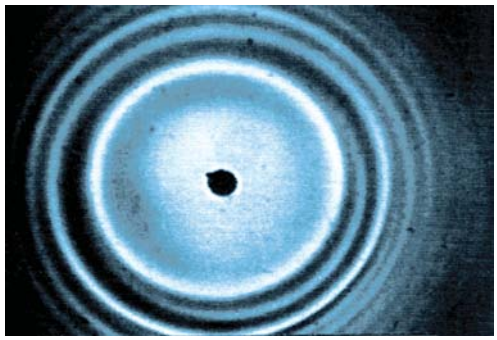

Figure 11

Pattern of capillary waves taken 5 ms after impact of a copper stick on an ethanol film of 1.4-mm thickness. The picture covers an area of about 25 mm × 35 mm. The maxima of the surface curvature in the depressions in the wave profile are seen as dark rings. From Yarin & Weiss (1995). Courstesy of Cambridge University Press.

such a pattern of inertial spreading counteracted by surface tension (Davidson 2002, Weiss & Yarin 1999). The weakest drop impacts, as well as slight perturbation by a solid body (e.g., a stick), induce a system of concentric waves propagating from the point of impact (**Figure 11**). On scales of the order of 1 mm, the gravity effect on the wave propagation is negligible, and the dynamics is due to the competition of inertia and surface tension. Yarin & Weiss (1995) showed that at a distance much larger than the impactor size (D of a drop or a stick), the waves are self-similar and the perturbation of the free surface $\chi(r, t)$, the liquid layer thickness being $h = h_0 (1 + \chi)$ (**Figure 11**), is described by the following expression:

$$\chi = \frac{2S}{\Gamma(1/4)} \frac{1}{\eta^{3/2}} \left[\cos\left(\frac{1}{4}\eta^2 + \frac{1}{8}\pi\right) + \sin\left(\frac{1}{4}\eta^2 + \frac{1}{8}\pi\right) \right] \tag{10}$$

Here the dimensionless S is a known impact intensity, $\Gamma(1/4) = 3.6256$ is the gamma function of the argument 1/4, and the self-similar variable η, which should be large, is given by

$$\eta = \frac{r}{(\alpha t)^{1/2}}, \tag{11}$$

where $\alpha = (\sigma h_0/\rho)^{1/2}$, i.e., wave crests and troughs propagate as $r \sim (\sigma h_0/\rho)^{1/4} t^{1/2}$. Different wave patterns shot at different time moments, like that of **Figure 11**, can be condensed into a single curve corresponding to Equation 10.

5. SPREADING, SPLASHING, RECEDING, AND REBOUND IN THE EXPERIMENTS ON DROP IMPACT ON A DRY SURFACE

Drop impacts on dry surfaces exhibit more complicated flow patterns than those on the wetted surfaces, due to the influence of the surface texture, i.e., wettability and roughness. The experiments of Rioboo et al. (2001) revealed six possible

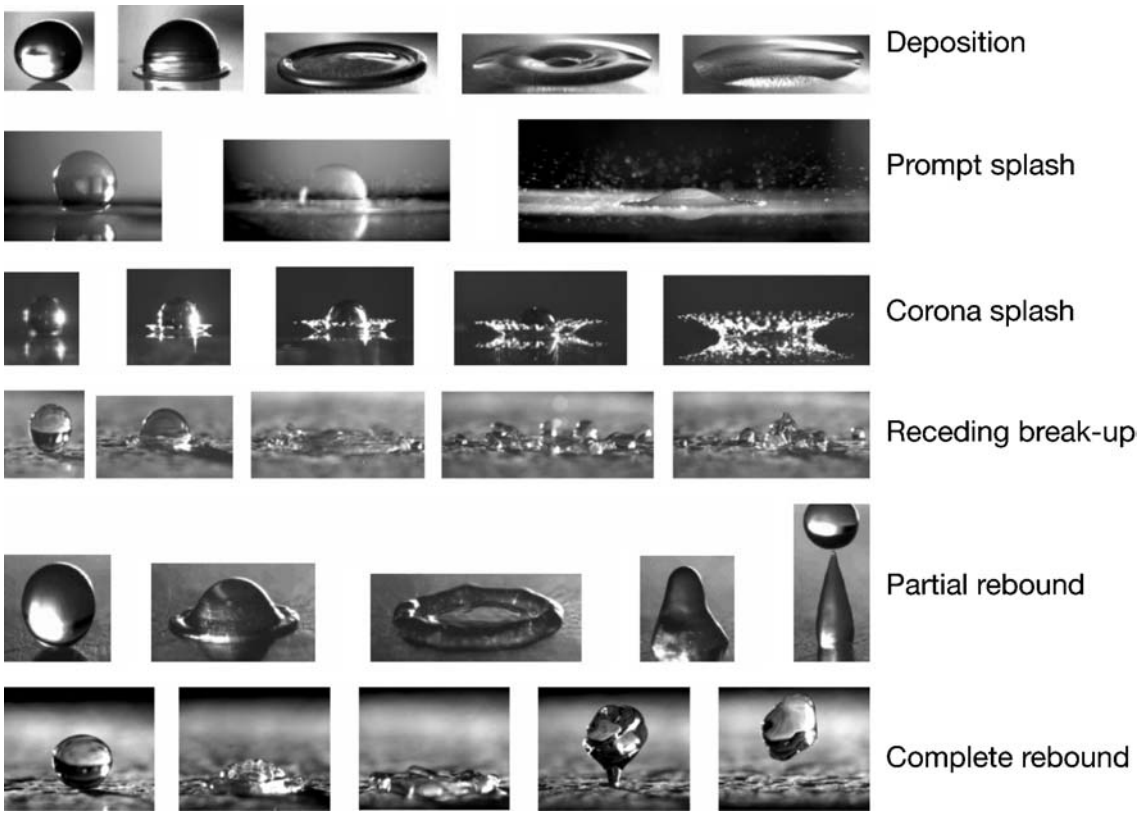

Figure 12

Morphology of drop impact on a dry surface. From Rioboo et al. (2001). Courtesy of Begell House.

outcomes of drop impact on a dry wall, shown in **Figure 12**. The deposition scenario consists of two stages: the kinematic and the actual deposition (Rioboo et al. 2002). In the kinematic stage the radius of the drop base $R \sim t^{1/2}$ is irrespective of the physical properties of the liquid and the surface. Dependence on these parameters begins to be felt only in the actual deposition stage. In both cases, at the end the drops spread over the surface and stay there, as, for example, on the top line of **Figure 12**. The ratio of the final lamella diameter at the wall to that of the drop, i.e., the maximum spread factor $\xi = 2R_{max}/D$, ranges from approximately 1.25 to 5 for different drop impacts resulting in deposition without recoil (Rioboo et al. 2002, Sikalo et al. 2002). Scheller & Bousfield (1995) proposed the empirical correlation

$$\xi = 0.61(\mathrm{Re}^2\mathrm{Oh})^{0.166} = 0.61\left(\frac{\mathrm{We}}{\mathrm{Oh}}\right)^{0.166} \qquad (12)$$

The first stage, and partly the second, constitute an initial phase of the other scenarios of drop impact on a dry surface illustrated in **Figure 12**. Additional factors come into play sooner or later, introducing new morphological features. The prompt splash scenario (second line from the top in **Figure 12**) is promoted by increased impact velocity on a rough surface, as a result of which tiny droplets are detached at the periphery of the liquid lamella generated by the spreading drop. At the end the impacting drop spreads and stays at the wall. As surface tension is reduced, the liquid lamella can detach from the wall, resulting in the corona splash scenario (third line from the top in **Figure 12**). The corona is reminiscent of the crowns recorded in splashes of drops on very thin liquid films by Wang & Chen (2000); these might be triggered by wall roughness that made their slopes distinct from those shown in **Figure 3*b*** (about 90°), but similar to the above in **Figure 12**. The corona splash can be completely suppressed by decreasing the pressure of the surrounding gas (Xu et al. 2005), which points at an important role of gas in triggering perturbations of the spreading lamella in addition to those due to the direct effect of wall roughness.

After the kinetic energy of drop impact has been partly dissipated by the viscous forces and partly converted into the surface energy associated with the greatly increased free-surface area, the subsequent behavior of the lamella depends largely on the surface wettability. The latter is characterized by the advancing and the receding contact angles, θ_{adv} and θ_{rec}, respectively, which can be measured by the sessile drop method at a certain velocity of the contact-line motion U, which is characterized by the capillary number $Ca = U\mu/\sigma$. Due to the contact angle hysteresis (if any), $\theta_{rec} < \theta_{adv}$ (without it $\theta_{rec} = \theta_{adv}$). The latter is due to the effect of wall roughness or chemical heterogeneities. For a given static drop volume a maximum (based on θ_{rec}) and a minimum (based on θ_{adv}) diameter, d_r and d_a respectively, can be defined, approximating drop shape as a truncated spherical cap (Rioboo et al. 2002)

$$\frac{d_i}{D} = 2\left[\frac{\sin^3\theta_i}{2\,(1-\cos\theta_i)\,\left(2-\cos\theta_i-\cos^2\theta_i\right)}\right]^{1/3} \tag{13}$$

where $d_i = d_r$ or d_a for $\theta_i = \theta_{rec}$ or θ_{adv}, respectively. Rioboo et al. (2002) and Schiaffino & Sonin (1997) argued that if the viscous effects dissipate most of the available kinetic energy, the slowly advancing lamella should attain the diameter d_a. By contrast, with a high level of kinetic energy, the diameter of the spreading lamella may overshoot d_r, after which the drop necessarily should begin to recede. Note that immediately after the overshoot the lamella shape should totally differ from a spherical cap, and the contact angle may be significantly larger than θ_{adv} because the contact-line motion was arrested mostly due to deceleration of the near-wall layer. A capillary wave should then be reflected from the drop front, leading to reduction of the contact angle, while the contact line is still at rest. For low-viscosity liquids the contact line will start its receding motion after a delay of the order of $(\rho D^3/\sigma)^{1/2}$ (i.e., several milliseconds for millimeter-size drops), still accompanied by capillary wave propagation over the lamella. When the receding motion of the shrinking lamella is sufficiently slow, it may be arrested at d_r, whereas at high receding velocities the lamella will pass through d_r and stabilize between d_r and d_a, all intermediate values of the contact angle between

θ_{rec} and θ_{adv} being possible due to the contact angle hysteresis. At this stage the receding breakup scenario (fourth line from the top in **Figure 12**) is characteristic of nonwettable surfaces (with $\theta_{adv} \to 180^\circ$ and $d_a \to 0$) and the shrinking lamella breaks up into a number of fingers, each of them also capable of further breakup, again probably due to the capillary instability.

The surface and the remaining kinetic energy in the liquid lamella at the end of the spreading stage may be sufficiently large not to be fully dissipated at the receding stage, with nonzero d_a passed through or $d_a = 0$ approached on a totally nonwettable surface. In such cases the receding velocity stays sufficiently high and the shrinking lamella virtually disappears near the impact point. The kinetic energy of such a collapse can still suffice to squeeze liquid upward from the surface, a rising liquid column reminiscent to some extent of the Worthington jet in **Figure 2*b***. It can stay partly at the surface and launch one or more droplets at its top due to the capillary instability (partial rebound scenario, fifth line from the top in **Figure 12**), or detach from the surface as an intact drop (complete rebound scenario, last line in **Figure 12**). Schiaffino & Sonin (1997) observed mercury drop rebound at a glass surface in the range of the impact Weber number $1.88 < We \leq 2.4$l; at $We < 1.88$ the mercury drops receded but stayed on the wall. Interestingly, jumps similar to the rebound scenario can be produced even without drop impact. In the experiments of Kirko et al. (1970) a mercury drop located on the bottom of a container filled with hydrochloric acid was initially squeezed by gravity. When the container was released from a drop tower, the gravity effect was actually "switched off" in flight. A camera mounted in the container showed the onset of receding motion (tending to recover the spherical shape) so vigorous that it resulted in full rebound and the drop jumped off the container bottom. Thus, the origin of drop deformation prior to the rebound (kinetic energy of impact or gravity squeezing) is immaterial.

Mundo et al. (1995) characterized the transition from spreading to splashing in drop impacts on dry surfaces at atmospheric pressure using the parameter $K_d = We^{1/2}\,Re^{1/4} = Oh\,Re^{5/4} = K^{5/8}$, i.e., a threshold value of $K = WeOh^{-2/5}$ was expected, which is similar to Equation 3. Note also that Stow & Hadfield (1981) proposed to use $WeOh^{-2/5}$ as a function of roughness to characterize the splashing threshold on dry surfaces, but it is not clear from their photography whether they were dealing with a corona-forming splash or with a prompt splash or perhaps fingering at the drop periphery. The splashing threshold by Mundo et al. (1995) was $K_{d,S} = 57.7$, i.e., $K_S = 657.48$. Cossali et al. (1997) proposed to correlate the available data on the splashing threshold at a dry surface at atmospheric pressure as

$$K_S = 649 + 3.76 \big/ R_{nd}^{0.63} \tag{14}$$

Range & Feuillebois (1998) argued that their experimental data on splashing threshold for normal drop impact on a dry surface, like those of Stow & Hadfield, can be described in terms of the critical Weber number We_S as a function of the surface roughness. Rioboo et al. (2001) claimed that the thresholds between the various scenarios in **Figure 12** cannot be quantified in terms of the dimensionless groups We, Re, Oh, and K of Equation 1—a clear manifestation that these dimensionless groups are insensitive to the wettability and roughness effects, which are of

Table 1 Summary of the effect of each parameter on each of the six scenarios, from Rioboo et al. (2001)*

Increase of	Deposition	Prompt splash	Corona splash	Receding breakup	Partial rebound	Complete rebound
V_0	↓	↑	↑	↑	↑	
D	↓	↑				
σ		↓	↓	↑	↑	↑
μ	↑	↓	↓	↓		
R_a	↓	↑	↓			
R_w		↓				
θ_{rec}				↑	↑	↑

*Arrows indicate the sense of the respective parameter change to exceed the threshold for that outcome.

the utmost importance in drop impacts on a dry surface. Accordingly, these authors opted to outline the trends indicated by variation of separate physical parameters, which include the roughness amplitude and wave length, R_a and R_w, respectively, and the wettability characteristic θ_{rec}. These trends are summarized in **Table 1**. Also note that the photographs presented in Range & Feuillebois (1998) demonstrate that they dealt not with corona splash but rather with the prompt splash scenario (cf. **Figure 12**).

Entrapment of a small air bubble under the center of the bottom of a drop impacting a solid dry surface was recorded in several experiments (Chandra & Avedisian 1991, Fujimoto et al. 2000, Qiao & Chandra 1996).

Experiments on drop impact on superhydrophobic surfaces are of great interest for many applications. Super water-repellant surfaces are highly rough and in some cases "fluffy"/fractal, which is achieved, for example, by anchoring long molecules or a dense forest of carbon nanotubes, or by depositing nonwoven polymer nanofiber mats using electrospinning. Drop impacts on them produce curious phenomena of bouncing (Lau et al. 2003, Rioboo et al. 2001, Schiaffino & Sonin 1997). On superhydrophobic substrates the contact-line hysteresis and the associated viscous losses are absent. In such cases normal drop impacts at low $We = 0.07$ lead to rebound of an almost spherical drop with a restitution coefficient of about 0.9 (Richard & Quere 2000). Details of the flow field at the spreading and receding stages after a stronger impact on a superhydrophobic surface at the higher $We = 18$ affect the outcome, leading to a partial rebound scenario similar to that of **Figure 12** rather than to complete rebound of a spherical drop (Richard & Quere 2000). After drop impact onto a superhydrophobic surface at $1 < We < 10$ capillary waves propagated over the free surface, creating drop shapes similar to the Aztec stepped pyramids or tori with a total dry out in the middle (Renardy et al. 2003). Clanet et al. (2004) showed that the maximum spread factor for bouncing low-viscosity drops on superhydrophobic substrates is given by $\xi = 0.9\ We^{1/4}$, which yields significantly lower values of ξ than Equation 12 because liquid inside such drops is far from being at rest at the moment the contact line is arrested.

Rebound is facilitated by elevated surface temperatures, especially when the Leidenfrost effect sets in and the drop is propelled upward by vapor at its base (Chandra & Avedisian 1991, Frohn & Roth 2000, and Rein 2002).

Drop impacts on inclined surfaces frequently lead to partial or complete rebound, which is enhanced at higher surface temperatures. In such cases there is a tendency to characterize the impact outcome in terms of the Weber number We_n based on the normal component of the impact velocity (Mundo et al. 1995).

The axisymmetric patterns of drop evolution during the kinematic and spreading phases are sometimes perturbed by azimuthal disturbances, whose growth results in fingering at the rim of a spreading drop on a dry wall. Detailed experimental studies of the fingering were conducted by Marmanis & Thoroddsen (1996) and by Thoroddsen & Sakakibara (1998) with water, water/glycerine, and alcohol/water mixtures, and by Aziz & Chandra (2000) with molten tin drops impacting stainless steel surfaces kept at temperatures below and above the melting point of tin. Marmanis & Thoroddsen counted the number of fingers seen on the splatter left behind after a colored drop impact on a thick rough linen paper. (No receding or rebound is possible in this case because the paper absorbs the liquids.) They correlated the data as

$$N_f = CRe^{3/8}\ We^{3/16} = C\left(\frac{We}{Oh}\right)^{3/8} \qquad (15)$$

The experimental results for drop impact on a glass surface (Thoroddsen & Sakakibara 1998) showed an increase in the number of fingers relative to that on a paper surface under comparable conditions. Range & Feuillebois (1998) found in their experiments that N_f depends on the roughness amplitude R_a (and shape) significantly; as R_a increased N_f decreased. Thus, the factor C in Equation 15 probably depends on surface wettability and roughness. However, the situation is even more complicated because the number of fingers is not constant during drop spreading: Splitting and merging of fingers were recorded by Thoroddsen & Sakakibara (1998). Aziz & Chandra (2000) counted the number of fingers on solidified tin splatters (solidification partially or completely prevents the receding and rebound stages). The effect of the surface temperature on the number of fingers was clearly visible, which means that the factor C in Equation 15 as a minimum should also depend on the drop and surface temperatures.

Recently, Rozhkov et al. (2002, 2004) reported experiments with drop impact on a small target (of a size comparable to D) where most of the liquid lamella is free and propagates in air rather than in contact with a solid wall. Free rims are formed at the far edges of the lamellae due to the surface tension and, moreover, develop patterns closely resembling those of the fingering.

6. MODELING OF DROP IMPACT ON A SOLID DRY SURFACE

For drop spreading on a dry surface without receding stage, the maximum spread factor ξ in many (but not all) cases can be accurately predicted using simple semiempirical analytical models based on the energy balance (Chandra & Avedisian 1991,

Mao et al. 1997, Pasandideh-Fard et al. 1996). The initial kinetic and surface energy partly dissipate, the remainder comprising the surface energy of the final deposit, assumed to be at complete rest. The deposit shape is assumed to be puddle-like, and the viscous dissipation is estimated with certain simplifying assumptions and on the basis of available empirical information. The calculated values of ξ agree fairly well with several sets of the experimental data (Mao et al. 1997, Pasandideh-Fard et al. 1996). For significant residual motion inside a drop after its contact line has been arrested, predictions of such models will be inaccurate. A review of several previous semiempirical models of drop spreading can be found in Bennett & Poulikakos (1993) and Scheller & Bousfield (1995).

The lubrication approximation equation is traditionally used to study the spreading of drops on partially or completely wettable surfaces (e.g., Clay & Miksis 2004, Ehrhard & Davis 1991, Starov et al. 1994). The approach allows relatively easy inclusion of certain complicating factors, e.g., those related to heat and mass transfer in the drop.

In cases where drop spreading is followed by the receding stage, the analytical approach is still possible but calls for a more elaborate dynamic model incorporating the fact that the spreading liquid lamella on the wall is surrounded by the free rim emerging due to the surface tension effect (Roisman et al. 2002b). The evolution of such a doughnut-like drop is actually determined by the free rim motion and its interaction with the spreading liquid lamella on the wall inside of it, as well as by the forces imposed on the rim by the wall. Roisman et al. (2002b) used the mass and momentum balance equations for the free rim, with allowance for the inertial, viscous, and surface tension forces and wettability effects. They showed that the simple analytical description resulting from the model is capable of rather accurate prediction of the evolution of the rim diameter up to its maximum, followed by its shrinkage during the receding stage. The model can be generalized to describe the collision of two spreading lamellae from two neighboring impacts (Roisman et al. 2002a). Such a collision results in an upward splash of colliding liquid elements from the wall.

Xu et al. (1998), Kim & Chun (2001), and Okumura et al. (2003) attempted to develop an analytical model of drop rebound. Xu et al. (1998) postulated that drop dynamics can be described by a damped spring-mass equation and tried to identify its coefficients semiempirically, with the real physical parameters involved. Okumura et al. (2003) used scaling arguments to prove that in the limit of small deformations drops behave as a spring-mass system. Because they considered a superhydrophobic surface, the effect of viscous damping could be disregarded. Kim & Chun (2001) employed and supplemented the energy balance with a simplified description of the drop shape throughout the impact process, with a cylinder or a truncated sphere as an approximation of the drop shape. In addition, a number of simplifying assumptions and the empirical information were used to evaluate the viscous dissipation. Their model, based on the cylindrical drop shape, was capable of describing the spreading and receding stages, as well as the onset of rebound in several experiments. Their model based on the truncated sphere shape was less successful.

The analytical description of drop spreading over a wettable wall based on simple scaling arguments about the momentum balance shows that even though there is

no impact velocity (the drop merely "settling" on the wall), the factor that initially limits the dynamics of spreading is inertia (Biance et al. 2004). This yields the drop base radius as $R \sim (\sigma D/\rho)^{1/4} t^{1/2}$, the result already mentioned in Section 4 for drops spreading on a thin liquid film. Subsequently, inertia is replaced by viscosity, and the wettability-driven spreading of an axisymmetric drop is described by Tanner's classical law $R \sim D[\sigma t/(\mu D)]^{1/10}$, the transition time between the two regimes being of the order of $(\rho\sigma D/\mu^2)^{1/8}(\rho D^3/\sigma)^{1/2}$ (Biance et al. 2004; see also Starov et al. 1994).

Besides the analytical modeling, several works are devoted to direct numerical simulation of drop spreading on dry, partially wettable surfaces. Fukai et al. (1993) used such simulations based on the finite element method. They solved the Navier-Stokes equations, dispensing with the no-slip condition at the moving contact line to alleviate the classical nonintegrable stress singularity. In fact, the only condition implemented at the contact line was that it moves parallel to the surface. Their results showed formation of characteristic doughnut-like shapes of the drop during its spreading as well as partial receding. In a later work, Fukai et al. (1995) improved this model by applying certain conditions at the moving contact lines. In particular, the measured values of the advancing and receding contact angles, θ_{adv} and θ_{rec}, were implemented at the contact lines in the code. As the drop reached its maximum spreading, the contact line was arrested, while the contact angle was changing from θ_{adv} to θ_{rec} before the receding stage began. Only during this transition were the no-slip boundary conditions implemented at the contact lines. Comparing the numerical predictions with the experimental data showed that shape evolution of spreading and receding drops is described accurately. Pasandideh-Fard et al. (1996) used the volume-of-fluid method to describe viscous drop spreading on a dry, partially wettable surface, with either constant or variable measured contact angles implemented at the contact line. The variable angles yielded a much more accurate prediction of the drop spreading radius R(t). Whereas previous works dealt with normal impact, Bussmann et al. (1999) and Pasandideh-Fard et al. (2002) tackled more complicated three-dimensional (3D) cases of the oblique impact and drop impact onto a sharp step. The time-dependent contact angles measured from the photographs were used in their code as the boundary conditions at the moving contact lines. The predicted drop shapes agreed fairly well with the experimental ones. In a later work, Bussmann et al. (2000) employed the same code to simulate the cases of normal impact, where drop spreading is followed by significant receding. In some cases the free rim at the edge of the receding liquid lamella at the wall develops perturbations and finger-like structures remained at the wall or broke up into secondary droplets after the rim had passed. The authors introduced artificial velocity perturbations in fluid near the wall shortly after the impact and demonstrated that this results in slight fingering (similar to prompt splash in **Figure 12**) at the spreading stage, and in strong fingering (receding breakup) at the receding stage. The predicted patterns were qualitatively similar to those in the experiments. The nature of the perturbations and their growth mechanism in the calculations were unrelated to any specific physical mechanism. Because the contact line receding proceeds at an almost constant velocity (Mourougou-Candoni et al. 1999) and perturbations can be triggered by the wall roughness, the receding rim should

also be subject to the cusp-and-jet formation mechanism similar to that on top of the crowns discussed in Sections 2 and 3, which may explain fingering at this stage.

Air entrapment between an oncoming drop and a solid wall was studied numerically by Mehdi-Nejad et al. (2003). In close agreement with experimental evidence, increased air pressure below the drop bottom resulted in a dent there, which became an entrapped bubble at the center of the deposited drop.

In general, the cases of drop spreading on a dry solid surface (versus splashing) imply significant viscous effects. Nevertheless, Davidson (2000) considered the problem an inviscid one and employed the boundary integral method to predict drop evolution, with a constant contact angle of 90° imposed at the moving contact line. The characteristic doughnut-like drop shapes with a visible free rim about the central lamella were predicted, which is not surprising because competition of the surface tension and inertia responsible for rim formation was accounted for. However, semiempirical modification of the results was called for to match the predicted drop spreading radius R(t) to the experimental data.

The boundary condition at the moving contact line in drop spreading on a dry, partially wettable surface deserves additional discussion. Very close to the wall the liquid motion is so slow due to the no-slip condition that molecular wettability-driven slip becomes dominant near the contact line. The contact line should then slowly slip over the wall, as it is well known for wettability-driven propagation (cf. Tanner's law for an axisymmetric drop with $R \sim t^{1/10}$). However, this slip is negligibly slow compared to the characteristic spreading velocities even in highly viscous drops, hence the free surface of the spreading drop should be strongly pulled forward by the macroscopic physical factors of the process (the kinetic energy of the drop impact, or the gravity force). On the other hand, at the lowest level of the drop contour (the contact line) it moves at a much lower speed resulting from the molecular mechanisms. In such circumstances severe deformation of the drop surface is expected near the contact line, with the attendant strong effect on the apparent contact angle and its evolution. Reznik & Yarin (2002a–c) simulated numerically gravity-driven squeezing of highly viscous drops on horizontal and inclined walls, or drop squeezing between two approaching plates, while implementing wettability-driven slip at the moving contact line; a similar approach was also implemented by Sikalo et al. (2005). The Stokes equations were solved using the boundary element method. Results showed that so long as the spreading process was sufficiently strong, the free surface near the contact line rapidly developed a 180° contact angle, i.e., rolling motion set in (cf. Dussan 1979). [Note that Betelu et al. (1997) assumed rolling motion in their numerical simulations of drop spreading from the very beginning of the process.] The predicted shapes of the spreading drops with rolling motion at the contact line agreed fairly well with the experimental data of Marino et al. (1996). Only at the later stage, when gravity-driven spreading had slowed down, did the contact-line motion approach the wettability-driven limit, although it was distinct from it as long as the bulk flow still affected the free-surface shape near the contact line. These results suggest that rolling motion at the contact line is an inevitable outcome of any sufficiently fast drop spreading process on a dry solid surface, which also eliminates the classical nonintegrable stress singularity. The data of Roux & Cooper-White

(2004) also suggest that for about 1.5 ms after the impact the advancing contact angle increases in time; the data of Sikalo et al. (2005) also show a similar trend. The data scattering, however, is significant and additional measurements are called for.

With spontaneous slow drop spreading on a fully wettable surface, a very thin precursor film precedes the apparent moving contact line, which similarly eliminates the stress singularity there (de Gennes 1985). The Molecular Dynamics (MD) models were recently used to simulate the dynamics of gravity- and wettability-driven spreading drops on fully and partially wettable surfaces, with and without an initial velocity (e.g., Gentner et al. 2004, He & Hadjiconstantinou 2003). The later work demonstrated that the drop base radius R(t) in the wettability-driven spreading on a fully wettable surface covered by a precursor film obeys Tanner's law, $R \sim t^{1/7}$, where the exponent 1/7 appears instead of 1/10, because planar drops were considered instead of axisymmetric ones. The corresponding dependence of the apparent contact angle on the velocity of the contact line (or on its dimensionless counterpart, the capillary number) was very close to the well-known experimental approximations. Gentner et al. (2004) used MD simulations for an axisymmetric drop impact with the initial velocities up to 18 m/s. They found $R \sim t^{1/2}$ immediately after an impact (which corresponds to the kinematic stage), replaced later on by $R \sim t^{1/7}$. The latter dependence signifies direct transition from the kinematic to the terminal wettability-driven stage, and also differs from Tanner's law for the axisymmetric case ($R \sim t^{1/10}$). However, it agrees with the Blake-Haynes molecular kinetic model. Note that MD simulations allow only consideration of nanometer-sized drops for about 10 ns and their predictions do not necessarily correspond to the phenomena characteristic of macroscopic drops.

Complicated pyramidal shapes of drops after impact on a superhydrophobic surface, and wavy shapes of solidifying solder drops with arrested contact lines, were successfully modeled via direct numerical simulations in Renardy et al. (2003) and in Waldvogel & Poulikakos (1997), respectively.

Theoretical treatment of fingering at the drop circumference following impact on a dry surface was frequently based on the idea of Rayleigh-Taylor-type instability. Allen (1975), who initiated this approach, considered the circumferential section of the drop surface moving radially outward and slowed down by friction forces from the solid surface. He suggested that the instability selects the fastest-growing perturbation, and its wave length $\lambda = 2\pi[3\sigma/(\rho a)]^{1/2}$ ("a" being the deceleration magnitude) dictates the number of fingers as $N_f = 2\pi R_{max}/\lambda$, where R_{max} is the final splat radius. Viscosity μ is not included directly in this analysis, but might affect the value of "a." However, no link between "a" and μ is provided and "a" can be taken as an average drop deceleration normal to the wall, $a \approx V_0^2/D$. Based on this model, and using an energy-based estimate of the drop spread factor, Bhola & Chandra (1999) predicted the number of fingers as $N_f = We^{1/2}Re^{1/4}/(4\sqrt{3}) = K^{5/8}/(4\sqrt{3})$ (cf. Equation 15). For the experimental evidence to match such a model, an average deceleration of the order of $a \sim 10^3 g$ (Aziz & Chandra 2000) is called for, which seems surprisingly high (Allen 1975). Also, the value of N_f used for comparison is the final number of fingers (subject to an agreed definition of a finger). The experiments of Thoroddsen & Sakakibara (1998), however, show that the final value of N_f cannot be traced directly back to the

initial number of fingers because of their splitting and merging effect not provided for in the linear Rayleigh-Taylor-type theory, which underlies this approach, hence the problematicity in comparing it with experimental data.

Kim et al. (2000) and Mehdizadeh et al. (2004) dispensed with the constant deceleration and extended the application of Rayleigh-Taylor-type instability further. They postulated that the unperturbed circumferential radius of the drop base varies as $R_0 = At^{1/2}$, "A" being a coefficient dependent on the impact conditions. This expression is actually only valid for the initial kinematic stage of drop spreading (see Section 5 and the beginning of the present Section), but Kim et al. (2000) extrapolated it over the whole spreading process. Then they considered planar potential source flow corresponding to the kinematics of $R_0(t)$ and introduced small perturbations of the circumferential radius and of the flow. The solved resulting linearized potential problem yielded the current shapes of the perturbed circumference with the instability as above related to the deceleration varying as $a = (A/4)t^{-3/2}$. The value of "a" fitting the splat patterns photographed in the above two works appears to be of the order of 10^5 g, which seems puzzling. To be consistent with the experimental data, the theory involves early time moments after the impact at which the flow near the drop base cannot be considered planar. Mehdizadeh et al. (2004) correlated their predictions for the number of fingers as $N_f = 1.14\ We^{1/2}$ (cf. Equation 15). The effect of surface roughness is totally disregarded in this approach in spite of the fact that higher roughness dramatically enhances fingering patterns (Prunet-Foch et al. 1998); Range & Feuillebois (1998) found an opposite trend: as R_a increased, N_f decreased.

Thoroddsen & Sakakibara (1998) suggested that Rayleigh-Taylor-type instability leading to fingering could be due to air entrapment under the oncoming drop. This idea has not been developed theoretically. The ideas proposed to describe instabilities arising near rapidly moving contact lines have not been applied to the fingering accompanying drop spreading on a dry solid surface (Range & Feuillebois 1998 and references therein), except for some encouraging estimates and comparisons in Prunet-Foch et al. (1998). The inertia-related jetting in the neck underneath a drop, similar to that described in Section 4 for impacts on liquid films, can also be expected on a solid surface. When accompanied by azimuthal (e.g., capillary) instability of the jet tip, such jetting could also result in fingering, especially at the early moments when such fingers are frequently recorded. The rim at the edge of the liquid lamella on the wall is also subject to cusp-and-jet formation (similar to the rims on top of the crowns discussed in Sections 2 and 3) or to the capillary instability enhanced by the inertia-related factors, which may result in fingering in certain cases (Range & Feuillebois 1998; Rozhkov et al. 2002, 2004). In their first work, Rozhkov et al. mentioned that their experimental data do not allow one to distinguish the dominant mechanism, and in both works they argued that either of the two may be responsible for triggering the rim nonuniformity. The fingers then grow due to rim deceleration, which causes lesser velocity reduction of the thicker rim sections than of the thinner ones. The results of Xu et al. (2005) suggest that surrounding gas can play a role also as a fingering trigger, and that fingering can be suppressed by decreasing the pressure. It seems that a plausible explanation of fingering still needs to be found.

7. CONCLUSIONS AND FUTURE DIRECTIONS

For a normal drop impact on a thin liquid layer (less than the drop diameter), we understand the nature of the transition to splashing, crown formation, and propagation, and are able to model these phenomena. Transition to splashing after an oblique impact still needs to be investigated, and models of crown propagation after such an impact still need to be verified experimentally. Impacts on extremely thin liquid films, where the effect of the surface roughness cannot be disregarded, deserve more thorough examination.

For normal impacts on a dry solid surface, full characterization of the effect of the surface texturing, i.e., wettability and roughness, on the drop evolution is still to be achieved, although significant experimental data are already available in the literature. The consequences of oblique impacts on dry surfaces are still insufficiently studied and understood.

Modeling of normal drop impacts on a dry surface resulting in spreading and deposition is reliable, although there is still no complete agreement on the boundary conditions to be implemented at the moving contact line. The transition from the spreading to the receding stage, where the contact line is arrested, is also still incompletely understood and poses significant obstacles to reliable modeling.

Drop bouncing from partly wettable and nonwettable superhydrophobic surfaces continues to be an active research area in both its experimental and theoretical aspects.

Formation of secondary droplets at the crown top and fingering at the free rim of the liquid lamella at the wall during the spreading and receding stages deserve further experimental and theoretical investigation to sort out the different ideas proposed to explain them. Regarding fingering, experiments at reduced pressure are called for.

Controlling drop deposition via modification of the fluid properties by means of various polymer admixtures has already borne some benefits in the agricultural context (Bergeron et al. 2000). Non-Newtonian rheological behavior is not confined to viscoelastic polymer solutions and characterizes a much wider family of fluids. At present, not much is known about drop impacts of numerous pseudoplastic, dilatant, and Bingham liquids (even paints!); cf. Nigen (2005). The same also applies to various thixotropic and rheopectic fluids with time-dependent rheological properties (due to flow-induced structural changes, rather than to temperature variation). Several such fluids represent particle suspensions or emulsions with possible flow-induced changes in the aggregate structure (Prunet-Foch et al. 1998). An additional example of impact with flow-induced property variation is that of drops with added surfactants (Cooper-White et al. 2002, Mourougou-Candoni et al. 1997, Zhang & Basaran 1997). In the presence of a surfactant, surface tension becomes flow- and time-dependent, which is referred to as the dynamic surface-tension effect. At sufficiently high concentrations, the surfactant molecules in the bulk self-organize themselves in rod-like or worm-like micelles. Such dilute and semidilute micellar solutions possess viscoelasticity since micelles act similarly to polymer macromolecules. In the strong stretching flow accompanying drop spreading, micelles are mechanically degraded and reassemble and provide significant viscoelastic resistance. This results in a combination of thixotropic-like behavior at the spreading stage, and rheopectic-like behavior at the

receding and rebound stages. Splashing threshold of a single impact on a pre-existing liquid film can be described with an expression similar to Equation 3*a* with the right-hand side depending not only on H, but also on the solution elasticity characterized by the Deborah number (Lampe et al. 2005). This demonstrates the kind of unusual phenomena that can be encountered once a wider family of complex and smart fluids is employed in drop impact studies.

Significant progress in our knowledge and understanding of drop-impact-related phenomena has been achieved over the years, beginning with the early works of Worthington more than a century ago. Prophecy, forecasts, and futurology are typically a thankless task, but the impetuous development of new technologies and the rapid progress in experimental techniques and in theoretical and numerical tools, together with our natural curiosity, make it relatively easy to predict that hydrodynamic research and insight into drop impacts will continue to be fascinating in the future.

ACKNOWLEDGMENTS

The author gratefully acknowledges his long-time research collaboration and numerous fruitful discussions with S.N. Reznik and D.A. Weiss, as well as the illustrations and photographs contributed by M. Rieber, R. Rioboo, and S. Thoroddsen. The discussions with C. Tropea and the comments of F. Maichle and R. Rioboo are gratefully appreciated.

LITERATURE CITED

Allen RF. 1975. The role of surface tension in splashing. *J. Colloid Interface Sci.* 51:350–51

Aziz SD, Chandra S. 2000. Impact, recoil and splashing of molten metal droplets. *Int. J. Heat Mass Trans.* 43:2841–57

Bennett T, Poulikakos D. 1993. Splat-quench solidification: estimating the maximum spreading of a droplet impacting a solid surface. *J. Mater. Sci.* 28:963–70

Bergeron V, Bonn D, Martin JY, Vovelle L. 2000. Controlling droplet deposition with polymer additives. *Nature* 405:772–75

Betelu S, Diez J, Thomas L, Gratton R, Marino B. 1997. A boundary element method for viscous gravity currents. *Int. J. Numer. Methods Fluids* 25:1–19

Bhola R, Chandra S. 1999. Parameters controlling solidification of molten wax droplets falling on a solid surface. *J. Mater. Sci.* 34:4883–94

Biance AL, Clanet C, Quere D. 2004. First steps in the spreading of a liquid droplet. *Phys. Rev. E* 69:016301

Bush JWM, Aristoff JM. 2003 The influence of surface tension on the circular hydraulic jump. *J. Fluid Mech.* 489:229–38

Bussmann M, Chandra S, Mostaghimi J. 2000. Modeling the splash of a droplet impacting a solid surface. *Phys. Fluids* 12:3121–32

Bussmann M, Mostaghimi J, Chandra S. 1999. On a three-dimensional volume tracking model of droplet impact. *Phys. Fluids* 11:1406–17

Chandra S, Avedisian CT. 1991. On the collision of a droplet with a solid surface. *Proc. R. Soc. London Ser. A* 432:13–41

Clanet C, Beguin C, Richard D, Quere D. 2004. Maximal deformation of an impacting drop. *J. Fluid Mech.* 517:199–208
Clay MA, Miksis MJ. 2004. Effects of surfactant on droplet spreading. *Phys. Fluids* 16:3070–78
Cooper-White JJ, Crooks RC, Boger DV. 2002. A drop impact study of worm-like viscoelastic surfactant solutions. *Colloid Surf. A* 210:105–23
Cossali GE, Coghe A, Marengo M. 1997. The impact of a single drop on a wetted solid surface. *Exp. Fluids* 22:463–72
Cossali GE, Marengo M, Coghe A, Zhdanov S. 2004. The role of time in single drop splash on thin film. *Exp. Fluids* 36:888–900
Davidson MR. 2000. Boundary integral prediction of the spreading of an inviscid drop impacting on a solid surface. *Chem. Eng. Sci.* 55:1159–70
Davidson MR. 2002. Spreading of an inviscid drop impacting on a liquid film. *Chem. Eng. Sci.* 57:3639–47
de Gennes PG. 1985. Wetting: statics and dynamics. *Rev. Mod. Phys.* 57:827–63
Dussan VEB. 1979. On the spreading of liquids on solid surfaces: static and dynamic contact lines. *Annu. Rev. Fluid Mech.* 11:371–400
Edgerton HE, Killian JR. 1954. *Flash! Seeing the Unseen by Ultra-High-Speed Photography*. Boston: Branford. 215 pp.
Ehrhard P, Davis SH. 1991. Non-isothermal spreading of liquid drops on horizontal plates. *J. Fluid Mech.* 229:365–88
Fedorchenko AI, Wang AB. 2004. On some common features of drop impact on liquid surfaces. *Phys. Fluids* 16:1349–65
Frohn A, Roth R. 2000. *Dynamics of Droplets*. Berlin: Springer-Verlag. 292 pp.
Fujimoto H, Shiraishi H, Hatta N. 2000. Evolution of liquid/solid contact area of a drop impinging on a solid surface. *Int. J. Heat Mass Trans.* 43:1673–77
Fukai J, Shiiba Y, Yamamoto T, Miyatake O, Poulikakos D, et al. 1995. Wetting effects on the spreading of a liquid droplet colliding with a flat surface: experiment and modeling. *Phys. Fluids* 7:236–47
Fukai J, Zhao Z, Poulikakos D, Megaridis CM, Miyatake O. 1993. Modeling of the deformation of a liquid droplet impinging upon a flat surface. *Phys. Fluids A* 5:2588–99
Fullana JM, Zaleski S. 1999. Stability of a growing end rim in a liquid sheet of uniform thickness. *Phys. Fluids* 11:952–54
Gentner F, Rioboo R, Baland JP, De Coninck J. 2004. Low inertia impact dynamics for nanodrops. *Langmuir* 20:4748–55
He G, Hadjiconstantinou NG. 2003. A molecular view of Tanner's law: molecular dynamics simulations of droplet spreading. *J. Fluid Mech.* 497:123–32
Josserand C, Zaleski S. 2003. Droplet splashing on a thin liquid film. *Phys. Fluids* 15:1650–57
Kim HY, Chun JH. 2001. The recoiling of liquid droplets upon collision with solid surfaces. *Phys. Fluids* 13:643–59
Kim HY, Feng ZC, Chun JH. 2000. Instability of a liquid jet emerging from a droplet upon collision with a solid surface. *Phys. Fluids* 12:531–41
Kirko IM, Dobychin EI, Popov VI. 1970. The phenomenon of the capillary bounce of a ball in weightlessness. *Dokl. USSR Acad. Sci.* 192:301–3 (In Russian)

Lampe J, DiLalla R, Grimaldi J, Rothstein JP. 2005. Impact dynamics of drops on thin films of viscoelastic wormlike micelle solutions. *J. Non-Newton. Fluid Mech.* 125:11–23

Lau KKS, Bico J, Teo KBK, Chhowalla M, Amaratunga GAJ et al. 2003. Superhydrophobic carbon nanotube forests. *Nanoletters* 3:1701–5

Lesser MB, Field JE. 1983. The impact of compressible liquids. *Annu. Rev. Fluid Mech.* 15:97–122

Levin Z, Hobbs PV. 1971. Splashing of water drops on solid and wetted surfaces: hydrodynamics and charge separation. *Philos. Trans. R. Soc. London Ser. A* 269:555–85

Mao T, Kuhn DCS, Tran H. 1997. Spread and rebound of liquid droplets upon impact on flat surfaces. *AIChE J.* 43:2169–79

Marino BM, Thomas LP, Diez JA, Gratton R. 1996. Capillary effects on viscous gravity spreadings of wetting liquids. *J. Colloid Interface Sci.* 177:14–30

Marmanis H, Thoroddsen ST. 1996. Scaling of the fingering pattern of an impacting drop. *Phys. Fluids* 8:1344–46

Mehdi-Nejad V, Mostaghimi J, Chandra S. 2003. Air bubble entrapment under an impacting droplet. *Phys. Fluids* 15:173–83

Mehdizadeh NZ, Chandra S, Mostaghimi J. 2004. Formation of fingers around the edges of a drop hitting a metal plate with high velocity. *J. Fluid Mech.* 510:353–73

Meier GEA, Klopper A, Grabitz G. 1992. The influence of kinematic waves on jet break down. *Exp. Fluids* 12:173–80

Mourougou-Candoni N, Prunet-Foch B, Legay F, Vignes-Adler M. 1999. Retraction phenomena of surfactant solution drops upon impact on a solid substrate of low surface energy. *Langmuir* 15:6563–74

Mourougou-Candoni N, Prunet-Foch B, Legay F, Vignes-Adler M, Wong K. 1997. Influence of dynamic surface tension on the spreading of surfactant solution droplets impacting onto a low-surface-energy solid substrate. *J. Colloid Interface Sci.* 192:129–41

Mundo C, Sommerfeld M, Tropea C. 1995. Droplet-wall collisions: experimental studies of the deformation and breakup process. *Int. J. Multiph. Flow* 21:151–73

Nigen S. 2005. Experimental investigation of the impact of an (apparent) yield-stress material. *At. Sprays* 15:103–17

Oguz HN, Prosperetti A. 1989. Surface-tension effects in the contact of liquid surfaces. *J. Fluid Mech.* 203:149–71

Okumura K, Chevy F, Richard D, Quere D, Clanet C. 2003. Water spring: a model for bouncing drops. *Europhys. Lett.* 62:237–43

Pasandideh-Fard M, Chandra S, Mostaghimi J. 2002. A three-dimensional model of droplet impact and solidification. *Int. J. Heat Mass Trans.* 45:2229–42

Pasandideh-Fard M, Qiao YM, Chandra S, Mostaghimi J. 1996. Capillary effects during droplet impact on a solid surface. *Phys. Fluids* 8:650–59

Prosperetti A, Oguz HN. 1993. The impact of drops on liquid surfaces and the underwater noise of rain. *Annu. Rev. Fluid Mech.* 25:577–602

Prunet-Foch B, Legay F, Vignes-Adler M, Delmotte C. 1998. Impacting emulsion drop on a steel plate: influence of the solid substrate. *J. Colloid Interface Sci.* 199:151–68

Qiao YM, Chandra S. 1996. Boiling of droplets on a hot surface in low gravity. *Int. J. Heat Mass Trans.* 39:1379–93
Range K, Feuillebois F. 1998. Influence of surface roughness on liquid drop impact. *J. Colloid Interface Sci.* 203:16–30
Rein M. 1993. Phenomena of liquid drop impact on solid and liquid surfaces. *Fluid Dyn. Res.* 12:61–93
Rein M. 2002. Interactions between drops and hot surfaces. In *Drop-Surface Interactions. CISM Courses and Lectures No. 456*, ed. M Rein, pp. 185–217. Vienna: Springer-Verlag. 314 pp.
Renardy Y, Popinet S, Duchemin L, Renardy M, Zaleski S et al. 2003. Pyramidal and toroidal water drops after impact on a solid surface. *J. Fluid Mech.* 484:69–83
Reznik SN, Yarin AL. 2002a. Spreading of a viscous drop due to gravity and capillarity on a horizontal or an inclined dry wall. *Phys. Fluids* 14:118–32
Reznik SN, Yarin AL. 2002b. Strong squeezing flow between parallel plates leads to rolling motion at the contact line. *Int. J. Multiph. Flow* 28:911–25
Reznik SN, Yarin AL. 2002c. Spreading of an axisymmetric viscous drop due to gravity and capillarity on a dry horizontal wall. *Int. J. Multiph. Flow* 28:1437–57
Richard D, Quere D. 2000. Bouncing water drops. *Europhys. Lett.* 50:769–75
Rieber M, Frohn A. 1999. A numerical study of the mechanism of splashing. *Int. J. Heat Fluid Flow* 20:455–61
Rioboo R, Bauthier C, Conti J, Voue M, De Coninck J. 2003. Experimental investigation of splash and crown formation during single drop impact on wetted surfaces. *Exp. Fluids* 35:648–52
Rioboo R, Marengo M, Tropea C. 2002. Time evolution of liquid drop impact onto solid, dry surfaces. *Exp. Fluids* 33:112–24
Rioboo R, Tropea C, Marengo M. 2001. Outcomes from a drop impact on solid surfaces. *At. Sprays* 11:155–65
Roisman IV, Prunet-Foch B, Tropea C, Vignes-Adler M. 2002a. Multiple drop impact onto a dry solid substrate. *J. Colloid Interface Sci.* 256:396–410
Roisman IV, Rioboo R, Tropea C. 2002b. Normal impact of a liquid drop on a dry surface: model for spreading and receding. *Proc. R. Soc. London Ser. A* 458:1411–30
Roisman IV, Tropea C. 2002. Impact of a drop onto a wetted wall: description of crown formation and propagation. *J. Fluid Mech.* 472:373–97
Roisman IV, Tropea C. 2005. Fluctuating flow in a liquid layer and secondary spray created by an impacting spray. *Int. J. Multiph. Flow* 31:179–200
Roux DCD, Cooper-White JJ. 2004. Dynamics of water spreading on a glass surface. *J. Colloid Interface Sci.* 277:424–36
Rozhkov A, Prunet-Foch B, Vignes-Adler M. 2002. Impact of water drops on small targets. *Phys. Fluids* 14:3485–501
Rozhkov A, Prunet-Foch B, Vignes-Adler M. 2004. Dynamics of a liquid lamella resulting from the impact of a water drop on a small target. *Proc. R. Soc. London Ser. A* 460:2681–704
Scheller BL, Bousfield DW. 1995. Newtonian drop impact with a solid surface. *AIChE J.* 41:1357–67

Schiaffino S, Sonin AA. 1997. Molten droplet deposition and solidification at low Weber numbers. *Phys. Fluids* 9:3172–87
Sikalo S, Marengo M. Tropea C, Ganic EN. 2002. Analysis of impact of droplets on horizontal surfaces. *Exp. Therm. Fluid Sci.* 25:503–10
Sikalo S, Wilhelm HD, Roisman IV, Jakirlic S, Tropea C. 2005. Dynamic contact angle of spreading droplets: experiments and simulations. *Phys. Fluids* 17:062103
Sivakumar D, Tropea C. 2002. Splashing impact of a spray onto a liquid film. *Phys. Fluids* 14:L85–88
Starov VM, Kalinin VV, Chen JD. 1994. Spreading of liquid drops over dry surfaces. *Adv. Colloid Interface Sci.* 50:187–221
Stow CD, Hadfield MG. 1981. An experimental investigation of fluid flow resulting from the impact of a water drop with an unyielding dry surface. *Proc. R. Soc. London Ser. A* 373:419–41
Taylor GI. 1959, The dynamics of thin sheets of fluid II. Waves on fluid sheets. *Proc. R. Soc. London Ser. A* 253:296–312
Thoroddsen ST. 2002. The ejecta sheet generated by the impact of a drop. *J. Fluid Mech.* 451:373–81
Thoroddsen ST, Etoh TG, Takehara K. 2003. Air entrapment under an impacting drop. *J. Fluid Mech.* 478:125–34
Thoroddsen ST, Etoh TG, Takehara K, Takano Y. 2004. Impact jetting by a solid sphere. *J. Fluid Mech.* 499:139–48
Thoroddsen ST, Sakakibara J. 1998. Evolution of the fingering pattern of an impacting drop. *Phys. Fluids* 10:1359–74
Thoroddsen ST, Takehara K. 2000. The coalescence cascade of a drop. *Phys. Fluids* 12:1265–67
Trujillo MF, Lee CF. 2001. Modeling crown formation due to the splashing of a droplet. *Phys. Fluids* 13:2503–16
Waldvogel JM, Poulikakos D. 1997. Solidification phenomena in picoliter size solder droplet deposition on a composite substrate. *Int. J. Heat Mass Trans.* 40:295–309
Wang AB, Chen CC. 2000. Splashing impact of a single drop onto very thin liquid films. *Phys. Fluids* 12:2155–58
Weiss DA, Yarin AL. 1999. Single drop impact onto liquid films: neck distortion, jetting, tiny bubble entrainment, and crown formation. *J. Fluid Mech.* 385:229–54
Worthington AM. 1908. *A Study of Splashes*. London: Longmans, Green. 129 pp.
Xu H, Liu Y, He P, Wang H. 1998. The TAR model for calculation of droplet/wall impingement. *J. Fluids Eng.* 120:593–97
Xu L, Zhang WW, Nagel SR. 2005. Drop splashing on a dry smooth surface. *Phys. Rev. Lett.* 94:184505
Yarin AL. 1993. *Free Liquid Jets and Films: Hydrodynamics and Rheology*. Harlow: Longman/New York: Wiley. 446 pp.
Yarin AL, Weiss DA. 1995. Impact of drops on solid surfaces: self-similar capillary waves, and splashing as a new type of kinematic discontinuity. *J. Fluid Mech.* 283:141–73
Zhang X, Basaran OA. 1997. Dynamic surface tension effects in impact of a drop with a solid surface. *J. Colloid Interface Sci.* 187:166–78

Annual Review of
Fluid Mechanics

Volume 38, 2006

Contents